

1 **Title:**

2 Extent and context dependence of pleiotropy revealed by high-throughput single-cell
3 phenotyping
4

5 **Author list:**

6 Kerry A Geiler-Samerotte^{a,b}

7 Shuang Li^a

8 Charalampos Lazaris^a

9 Austin Taylor^a

10 Naomi Ziv^a

11 Chelsea Ramjeawan^a

12 Annalise B Paaby^c

13 Mark L Siegal^a

14

15 **Author affiliations:**

16 ^a Center for Genomics and Systems Biology, Department of Biology, New York
17 University, New York, NY 10003

18 ^b Center for Mechanisms of Evolution, Biodesign Institutes, School of Life Sciences,
19 Arizona State University, Tempe, AZ 85287

20 ^c School of Biological Sciences, Georgia Institute of Technology, Atlanta, GA 30332

21

22 **Corresponding author:**

23 Kerry Geiler-Samerotte: kerry.samerotte@asu.edu

24

25

26

27

28

29

30

31

32

33

34

35

36

37

38

39

40

41

42

43 **Abstract:**

44 Pleiotropy – when a single mutation affects multiple traits – is a controversial topic with
45 far-reaching implications. Pleiotropy plays a central role in ongoing debates about how
46 complex traits evolve and whether biological systems tend to be modular or organized
47 such that every gene has the potential to affect many traits. Pleiotropy is also critical to
48 initiatives in evolutionary medicine that seek to trap infectious microbes or tumors by
49 selecting for mutations that encourage growth in some conditions at the expense of
50 others. Research in these fields, and others, would benefit from understanding the extent
51 to which pleiotropy reflects inherent relationships among phenotypes that correlate no
52 matter the perturbation (vertical pleiotropy), versus the action of genetic changes that
53 impose correlations between otherwise independent traits (horizontal pleiotropy). We
54 tackle this question by using high-throughput single-cell phenotyping to measure
55 thousands of pairwise trait correlations across hundreds of thousands of cells representing
56 hundreds of genotypes of the budding yeast, *Saccharomyces cerevisiae*. We map
57 pleiotropic quantitative trait loci using genotypes derived from a cross between natural
58 strains, and we separate vertical and horizontal pleiotropy by partitioning trait
59 correlations into within- and between-genotype correlations. We investigate how
60 pleiotropy can change by using genotypes from mutation-accumulation lines that
61 experienced minimal selection, and by tracking trait correlations through the cell-division
62 cycle. We find ample evidence of both vertical and horizontal pleiotropy, and observe
63 that trait correlations depend on both genetic background and cell-cycle position. Our
64 results suggest a nuanced view of pleiotropy in which trait correlations are highly context
65 dependent and biological systems occupy a middle ground between modularity and
66 interconnectedness. These results also suggest an approach to select pairs of traits that are
67 more likely to remain correlated across contexts for applications in evolutionary
68 medicine.

69
70
71
72
73
74
75
76
77
78
79
80
81
82
83
84
85
86
87
88

89 Introduction

90 Pleiotropy exists when a single mutation affects multiple traits [1,2]. Often,
91 pleiotropy is defined instead as a single gene contributing to multiple traits, although
92 what is implied is the original definition — that a single change at the genetic level can
93 have multiple consequences at the phenotypic level [2]. As our ability to survey the
94 influence of genotype on phenotype improves, examples of pleiotropy are growing [3-7].
95 For example, individual genetic variants have been associated with seemingly disparate
96 immune, neurological, and digestive symptoms in humans and mice [8,9]. Genes
97 affecting rates of cell division across diverse environments and drug treatments have been
98 identified in microbes and cancers [10,11]. A view emerging from genome-wide
99 association studies is that variation in complex traits is “omnigenic” in the sense that
100 many loci indirectly contribute to variation in many traits [12,13].

101
102 However, the extent of pleiotropy remains a major topic of debate because,
103 despite its apparent prevalence, pleiotropy is thought to be evolutionarily
104 disadvantageous. The more traits a mutation affects, the more likely it is that the mutation
105 will have a negative impact on at least one. Pervasive pleiotropy should therefore
106 constrain evolution [14], exacting what is known as a cost of complexity or cost of
107 pleiotropy [10,15-18]. This cost may bias which mutations underlie adaptation, for
108 example, toward less-pleiotropic *cis*-regulatory changes over more-pleiotropic changes in
109 *trans*-acting factors [19,20], or toward changes to proteins that participate in relatively
110 few biological processes [21,22]. Over long periods, the cost of pleiotropy may influence
111 the organization of biological systems, favoring a modular structure in which genetic
112 changes influencing one group of traits have minimal impact system-wide [23-28].

113 At stake in the ongoing debate about the extent of pleiotropy [29-32] are some of
114 modern biology’s prime objectives, including the prediction of complex phenotypes from
115 genotype data [17,33,34] and the prediction of how organisms will adapt to
116 environmental change [35,36]. These predictions are more challenging if genetic changes
117 influence a large number of traits with complex interdependencies. Nonetheless,
118 understanding how a given mutation influences multiple traits could be powerful,
119 allowing prediction of some phenotypic responses given others [37,38]. Indeed, recent
120 strategies in medicine called evolutionary traps aim to exploit pleiotropy, for example by
121 finding genetic changes that provide resistance to one treatment while promoting
122 susceptibility to another [39-41].

123 The lack of consensus about the extent of pleiotropy in natural systems is in part
124 due to poorly defined expectations for how to test for it experimentally. One key issue is
125 that defining a phenotype is not trivial [42,43]. Consider a variant in the *apolipoprotein B*
126 gene that increases low-density lipoprotein (LDL) cholesterol levels as well as the risk of
127 heart disease. Elevated LDL promotes heart disease [44], so are these two phenotypes or
128 one? Alternatively, consider a mutation in the *phenylalanine hydroxylase* gene that
129 affects nervous system function and skin pigmentation. These dissimilar effects, both
130 symptoms of untreated phenylketonuria (PKU), originate from the same problem: a
131 deficiency in converting phenylalanine to tyrosine [45]. Is it fair to call mutations that
132 have this single metabolic effect pleiotropic? Likewise, shall one call pleiotropic a
133 mutation that makes tomatoes both ripen uniformly and taste bad, when the effect of the

134 mutation is to reduce the function of a transcription factor that promotes chloroplast
135 development, which in turn necessarily affects both coloration and sugar accumulation
136 [46]?

137 The LDL, PKU and tomato cases are examples of vertical pleiotropy, *i.e.*
138 pleiotropy that results when one phenotype influences another or both are influenced by a
139 shared factor [4,42]. The alternative to vertical pleiotropy is horizontal pleiotropy, in
140 which genetic differences induce correlations between otherwise independent
141 phenotypes. It might be tempting to discard vertical pleiotropy as less “genuine” [47] or
142 less important than horizontal pleiotropy, but that would be a mistake because vertical
143 pleiotropy reveals important information about the underlying biological systems that
144 produce the phenotypes in question. Consider the value in identifying yet-unknown
145 factors in heart disease by finding traits that correlate with it, or in understanding where
146 in a system an intervention is prone to produce undesirable side effects. Consider also
147 that the extent and nature of vertical pleiotropy speak directly to the question of
148 modularity: modularity is implied if vertical pleiotropy either is rare or manifests as small
149 groups of correlated traits that are isolated from other such groups. If there is modularity
150 then there can be horizontal pleiotropy, when particular genetic variants make links
151 between previously unconnected modules.

152 The above considerations suggest that a unified analysis that distinguishes and
153 compares horizontal and vertical pleiotropy is needed to make sense of the organization
154 and evolution of biological systems. However, existing methods of distinguishing
155 horizontal and vertical pleiotropy are problematic because judgments must be made about
156 which traits are independent from one another. Such judgments differ between
157 researchers and over time. Indeed, the tomato example can be viewed as a case of
158 horizontal pleiotropy transitioning recently to vertical pleiotropy as knowledge of the
159 underlying system advanced.

160 In this study, we propose and apply an empirical and analytical approach to
161 measuring pleiotropy that relies far less on subjective notions of what constitutes an
162 independent phenotype. The key principle is that the distinction between vertical and
163 horizontal pleiotropy lies in whether traits are correlated in the absence of genetic
164 variation [42]. For vertical pleiotropy, the answer is yes: because one trait influences the
165 other or the two share an influence, non-genetic perturbations that alter one phenotype are
166 expected to alter the other. For horizontal pleiotropy, the answer is no: genetic variation
167 causes the trait correlation. In this study, we determined how traits correlate in the
168 absence of genetic variation by measuring single-cell traits in clonal populations of cells.

169 We used high-throughput morphometric analysis [48-52] of hundreds of
170 thousands of single cells of the budding yeast *Saccharomyces cerevisiae* to measure how
171 dozens of cell-morphology traits (thousands of pairs of traits) co-vary within clonal
172 populations and between such populations representing different genotypes. Within-
173 genotype correlations report on vertical pleiotropy, whereas between-genotype
174 correlations report on horizontal pleiotropy to the extent that they exceed the
175 corresponding within-genotype correlations. For one set of genotypes, we used 374
176 progeny of a cross of two natural isolates [53], which enabled not only the estimation of

177 vertical and horizontal pleiotropy but also the identification of quantitative trait loci
178 (QTL) with pleiotropic effects. For another set of genotypes, we used a collection of
179 mutation-accumulation lines, each of which contains a small number of unique
180 spontaneous mutations [54,55], which enabled a more direct test of the ability of
181 mutations to alter trait correlations.

182 The traits we study – morphological features of single cells – represent important
183 fitness-related traits [50,56,57] that contribute to processes such as cell division and
184 tissue invasion (*e.g.* cancer metastasis [58]). Cell-morphological features may correlate
185 across cells for a variety of vertical or horizontal reasons. Vertical reasons include: (1)
186 inherent geometric constraints (*e.g.* on cell circumference and area); (2) constraints
187 imposed by gene-regulatory networks (*e.g.* if the genes influencing a group of traits are
188 all under control of the same transcription factor); and (3) constraints induced by
189 developmental processes (*e.g.* as a yeast cell divides or “buds”, many morphological
190 features are affected). Horizontal pleiotropy might be evident because genetic variants
191 affecting two or more traits (that are otherwise weakly correlated) are segregating in the
192 progeny of the cross between two natural isolates. Alternatively, horizontal pleiotropy
193 might be evident because a particular allele strengthens the trait correlation so that
194 genetic variation affecting one trait is more likely to affect another when that allele is
195 present. These alternatives can be distinguished by examining trait correlations in two
196 subsets of progeny strains defined by which natural isolate’s allele they possess at a QTL
197 of interest.

198 In addition to genetic variation, non-genetic variation may also alter the
199 correlations between traits. We rely on non-genetic heterogeneity within clonal
200 populations to serve as perturbations that reveal inherent trait correlations. However, the
201 correlations themselves might be heterogeneous within these populations. For example,
202 the dependencies between morphological features may change as cells divide. To control
203 for this possibility, we performed our trait mapping and subsequent analysis after binning
204 cells into three stages (unbudded, small-budded and large-budded cells). We further
205 examined whether trait correlations change across the cell cycle by using a machine-
206 learning approach to more finely bin the imaged cells into 48 stages of division.

207
208 Collectively, the results we present here demonstrate that both types of pleiotropy,
209 vertical and horizontal, are prevalent for single-cell morphological traits, suggesting that
210 biological systems occupy a middle ground between extreme modularity and extreme
211 interconnectedness. Perhaps more surprisingly, we find that trait correlations are often
212 context dependent, and can be altered by mutations as well as cell-cycle state. The
213 dynamic nature of trait correlations at these different timescales encourages caution when
214 attempting to quantify and interpret the extent of pleiotropy in nature or when making
215 predictions about correlated phenotypic responses to the same selection pressure, as is
216 done when crafting evolutionary traps. However, applying our approach may suggest
217 which trait correlations are less context dependent and therefore more useful in setting
218 such traps.

219
220

221 **Results:**

222

223 ***QTLs with pleiotropic effects influence yeast single-cell morphology***

224 To detect genes with pleiotropic effects on cell morphology, we measured 167
225 single-cell morphological features (*e.g.* cell size, bud size, bud angle, distance from
226 nucleus to bud neck; **Table S1**) in 374 yeast strains that were generated in a previous
227 study from a mating between two wild yeast isolates [53,59]. These wild isolates, one
228 obtained from soil near an oak tree, the other from a wine barrel, differ by 0.006 SNPs
229 per site [60] and have many heritable differences in single cell morphology [61]. For
230 example, we find that yeast cells from the wine strain, on average, are smaller, are
231 rounder, and have larger nuclei during budding than yeast cells from the oak strain (**Fig**
232 **S1**).

233 To measure their morphologies, we harvested exponentially growing cells from
234 three replicate cultures of each of these 374 recombinant strains, and imaged on average
235 800 fixed, stained cells per strain using high-throughput microscopy in a 96-well plate
236 format (**Fig S2**). We used control strains present on each plate to correct for plate-to-plate
237 variation (see *Methods*), and quantified morphological features using CalMorph software
238 [52], which divides cells into three categories based on their progression through the cell
239 cycle (*i.e.* unbudded, small-budded, and large-budded cells) and measures phenotypes
240 specific to each category. Using 225 markers spread throughout the genome [53] and
241 Haley-Knott regression implemented in the R package R/qtl [62,63], we identified 44
242 QTL that contribute to variation in 158 of the surveyed morphological features (FDR =
243 5%; **Fig 1A**; **Table S1**). Most (37) of the QTL we detected are pleiotropic, meaning each
244 contributes to variation in more than one morphological feature (**Fig 1A**). The median
245 number of traits to which each QTL contributes is six.

246

247 ***Single genes with pleiotropic effects influence yeast single-cell morphology***

248 When a QTL affects multiple traits, it might not mean that variation in a single
249 gene is contributing to variation in these traits but instead that linked genes are
250 contributing to variation in distinct, individual traits. For several QTL with high
251 pleiotropy (highlighted in **Fig 1A**), we sought to test whether the effects on different
252 morphological features were due to the action of a single gene. We performed these tests
253 by swapping the parental versions of candidate genes (*i.e.* we genetically modified the
254 wine strain to carry the oak version of a given gene, and vice versa). We used the *delitto*
255 *perfetto* technique to perform these swaps [64], such that the only difference between a
256 parental genome and the swapped genome is the coding sequence of the single candidate
257 gene plus up to 1 kb of flanking sequence (see *Methods*). Candidate genes were selected
258 based on descriptions of the single-cell morphologies of their knockout mutants [65] and
259 the presence of at least one non-synonymous amino acid difference between the wine and
260 oak alleles [61].

261

262 When a candidate gene contributes to the morphological differences between the
263 wine and oak parents, we expect yeast strains that differ at only that locus to recapitulate
264 some of the morphological differences between the wine and oak parents. Indeed, this is
265 what we observe for *PXLI*, a candidate for the QTL on chromosome 11, and *HOF1*, a
266 candidate for the QTL on chromosome 13 (**Fig 1B**; compare each plot on the right to the
leftmost plot; see also **Table S2**). This influence is most pervasive for *HOF1*; both the

267 oak and the wine alleles have a strong effect on the morphology of the opposite parent,
268 and their effects recapitulate the parental difference to a large extent. The pervasive
269 influence of *HOF1* on various morphological features is consistent with the fact that this
270 gene's product affects actin-cable organization and is involved in both polar cell growth
271 and cytokinesis [66]. The effect of *PXLI* on cell morphology is also apparent across
272 many single-cell features, although only the oak allele has a strong effect that
273 recapitulates the parental difference. We evaluated *RASI*, a candidate for the QTL on
274 chromosome 15, but initial tests indicated that it did not have a significant impact on
275 most morphological features (**Table S2**). We also attempted to swap alleles for a
276 candidate gene corresponding to the QTL on chromosome 8, but were unsuccessful (see
277 *Methods*).

278 A previous screen for QTL influencing single-cell morphology in the progeny of a
279 genetically distinct pair of yeast strains (a different vineyard strain and a laboratory
280 strain) found some of the same pleiotropic QTL that we detect in the wine and oak cross
281 [67] (compare their Table 2 to our **Table S1**). In particular, we both find a QTL in the
282 same position on chromosome 15 that influences many morphological features related to
283 nucleus size, shape, and position in the cell (**Fig 1A**; orange). We also both detect a QTL
284 near base pair 100,000 on chromosome 8 that influences cell size and shape (**Fig 1A**;
285 pink). In the previous screen, the genetic basis of this QTL was shown to be a single
286 nucleotide change within the *GPAI* gene [67].

287 The main conclusion from our gene-swapping experiments, which is consistent
288 with the previous cell-morphology QTL study [67] as well as with comprehensive
289 surveys of how gene deletions affect the morphology of a laboratory yeast strain [10,48],
290 is that genes with pleiotropic effects on cell morphology are common in budding yeast.
291 Moreover, the morphological traits involved were previously shown to influence fitness
292 [50,56,57], which raises the question: why do so many genetic analyses (including ours)
293 detect pleiotropy [4,8-11,13] when other work suggests that pleiotropy exacts a cost
294 [16,17,19,20]?

295

296 *Dissecting pleiotropy using clonal populations of cells*

297 One hypothesis to explain pervasive pleiotropy may be that the phenotypes we
298 chose to measure are not independent. Instead, many of these single-cell morphological
299 features may be inherently related such that perturbing one will have unavoidable
300 consequences on another and thus any associated limitation of adaptation will be
301 unavoidable as well. In other words, the hypothesis is that much of the pleiotropy we
302 observe is vertical pleiotropy. A test of this hypothesis is to ask whether traits are
303 correlated in the absence of genetic differences. Our dataset provides a unique
304 opportunity to perform such a test because we quantified single-cell traits for, on average,
305 800 clonal cells per yeast strain (**Fig S2**).

306 We can leverage the hierarchical structure and large sample size of our dataset to
307 obtain precise estimates of the correlations that exist within and between strains, and
308 thereby to distinguish vertical from horizontal pleiotropy. Because we are studying clonal
309 families without a complicated pedigree structure, these within- and between-strain
310 correlations are equivalent to the so-called environmental and genetic correlations of
311 quantitative genetics [68]. Here, we use a simple (and fast) method that is appropriate for
312 two-level hierarchical data to partition the total correlation into a pooled within-strain

313 component (r_W) and a between-strain component (r_B) [69]. One caveat of this correlation-
314 partitioning approach is that r_B is effectively the correlation between strain means, which
315 can bias estimates of genetic covariance [68]. This bias is most pronounced at small
316 sample sizes [68], so our large sample sizes allay concern. Nonetheless, for a subset of
317 traits, we tested whether estimates obtained from correlation partitioning are similar to
318 those obtained from mixed-effect linear models that specify the variance-covariance
319 structure of the experimental design. Environmental correlations estimated using both
320 methods are nearly identical (**Fig S3**). Genetic correlations estimated by correlation
321 partitioning are sometimes slightly smaller in magnitude than those obtained by linear
322 modeling (**Fig S3**). This bias is conservative; it may prevent us from identifying cases
323 where the environmental and genetic correlations significantly differ but will not tend to
324 create such cases. Despite this reduced power, we rely on the correlation-partitioning
325 approach, which is substantially faster, because our goal is to estimate environmental and
326 genetic correlations for thousands of trait pairs.

327 Unlike the mapping analysis, which considered phenotypes across all three
328 classes of cell type (unbudded, small-budded and large-budded), this correlation-
329 partitioning analysis can only be applied to pairs of phenotypes measured in the same cell
330 type. Two of the 37 pleiotropic QTL exclusively affect traits from different cell types: a
331 QTL on chromosome 8 affects the short-axis length of unbudded cells and the short-axis
332 length of large-budded cells, and a QTL on chromosome 7 affects the cell axis ratio of
333 small-budded cells and the bud axis ratio of large-budded cells. The correlations for the
334 trait pairs affected by these two QTL cannot be partitioned because the traits are not
335 measured in the same cells within strains. Excluding these two QTL leaves 35 pleiotropic
336 QTL collectively contributing to 5645 pairs of traits (378, 1081, and 4186 pairs of
337 morphological features pertaining to unbudded, small-budded, and large-budded cells
338 respectively). For each of these trait pairs, we partitioned the correlation between traits.
339 In the analyses that follow, when we refer to r_W or r_B , we mean the magnitudes of these
340 correlations, as the sign has no relevance for arbitrary pairs of traits.

341

342 *Inherent relationships between traits contribute to pleiotropy*

343 We focus first on vertical pleiotropy by analyzing correlations that exist in the
344 absence of any genetic differences (r_W). The distribution of r_W values reflects the extent
345 of vertical pleiotropy, and the overall pattern of r_W values (*i.e.*, whether there are isolated
346 clusters of highly correlated traits versus a densely interconnected network of traits)
347 reflects the modularity of the underlying biological system. These within-strain
348 correlations are estimated with extremely high precision because of our large sample size
349 of hundreds of thousands of clonal cells (800 per each of 374 strains).

350 Most pairs of single-cell morphological traits are not strongly correlated across
351 clonal cells (**Fig 2A**). Median r_W is < 0.1 , and 74% of pairs have $r_W < 0.2$. Even if we
352 allow for nonlinear correlations by transforming data using a nonparametric model that
353 finds the fixed point of maximal correlation [70], r_W is less than 0.2 for roughly 65% of
354 pairs. These observations suggest that most of the morphological traits we surveyed are
355 not inherently related; *i.e.* for any individual cell, the value of one trait does not predict
356 well the values of most other traits.

357 Nonetheless, the distribution of r_W has a prominent right tail (**Fig 2A**) indicating
358 that some morphological features are strongly correlated across clonal cells. These

359 correlated features are more likely to be influenced by pleiotropic QTL. Among pairs
360 represented by this right tail (specifically, those with $r_w > 0.2$), 78% consist of traits that
361 share at least one QTL influence; the same is true for only 40% of pairs with $r_w < 0.2$.
362 Further, the number of pleiotropic QTL influencing both traits in a pair correlates with
363 that pair's r_w (Pearson's $r = 0.52$). This result suggests that some of the pleiotropy we
364 observe is vertical and results from inherent correlations that cause genetic perturbations
365 to one morphological trait to have consequences on another.

366 Next, we asked how many pleiotropic QTL act exclusively via vertical
367 pleiotropy—that is, how many QTL, identified across genotypes, are only associated with
368 traits that correlate highly within genotypes. Of the 35 pleiotropic QTL that we
369 examined, 11 exclusively influence traits with $r_w > 0.2$ (**Fig 2B**). For example, a QTL on
370 chromosome 10 influences a single pair of traits – the area of the nucleus and the length
371 of the nucleus in large-budded cells – with an r_w of 0.9, suggesting that the aspect ratio
372 of the nucleus is constrained by vertical pleiotropy (**Fig 2B**). Another QTL on
373 chromosome 16 exclusively influences traits corresponding to unbudded cells, all with r_w
374 > 0.4 (**Fig 2B**). Excluding these 11 QTL, nearly all (21) of the remaining 24 QTL have a
375 median r_w for the pairs of traits they influence that is higher than the median r_w given by
376 all possible pairs of traits (**Fig 2C**, compare All QTL to All Pairs). In sum, pairs of traits
377 with stronger correlations across clones (higher r_w) are disproportionately represented
378 among those influenced by pleiotropic QTL, suggesting that vertical pleiotropy drives a
379 large portion of the pleiotropy we detect.

380 Next, we investigated the organization of the biological system underlying cell
381 morphology by using network analysis to move beyond pairwise comparisons and ask if
382 morphological traits tend to be clustered into modules. Traits with higher r_w do indeed
383 tend to group into clusters in networks in which the single-cell morphological traits are
384 nodes and the r_w magnitudes are edge weights (**Fig 2D** shows the network for traits of
385 large-budded cells). This need not have been the case; single pairs of traits with high r_w
386 could have been distributed throughout the network without necessarily being clustered
387 near other high r_w pairs. Instead, networks representing single-cell morphological
388 features demonstrate more clustering than do random networks drawn from the same
389 values of r_w (**Fig 2E**; for corresponding figures from unbudded and small-budded trait
390 networks, see **Fig S4**). This observation might indicate that morphological phenotypes
391 have a modular organization, whereby phenotypes within a module exert influence on
392 one another, but exert less influence on phenotypes from other modules. However, this
393 observation could also result from human bias when enumerating phenotypes that can be
394 measured, in the sense that phenotypes that bridge modules might somehow be absent
395 from the data set. The comprehensive nature of CalMorph diminishes this concern. A
396 related concern is that apparent modules are formed by trivially related phenotypes, such
397 as the radius and diameter of a circular object, but we do not find such trivial
398 relationships among the CalMorph phenotypes. Even a high correlation between the
399 length and area of the nucleus, as noted above, implies a constraint on nuclear aspect
400 ratio.

401 Some pleiotropic QTL tend to influence traits that are clustered in these networks.
402 Even when we focus on the 24 pleiotropic QTL that do not exclusively influence traits
403 with high r_w , we find that more influence traits with higher weighted clustering
404 coefficients (wcc) than expected given the distribution of wcc across all traits (**Fig 2F**,

405 compare All QTL to All Pairs). For example, the QTL containing the *HOF1* gene has a
406 slight tendency to influence traits with higher than average *wcc* (**Fig 2D**: purple nodes;
407 **Fig 2F**: purple points).

408 Together, these observations (**Fig 2**) suggest that natural genetic variation
409 contributing to the single-cell morphological features we measured often acts via vertical
410 pleiotropy. In other words, correlations among morphological features that are present in
411 the absence of genetic variation underlie a large portion of pleiotropic genetic influences
412 on single cell morphology. Still, there are hints of another mechanism at play. Some QTL
413 tend to influence traits that are among the most weakly clustered in the correlation
414 network (**Fig 2F**). Moreover, most of the pleiotropic QTL we surveyed (24/35) each
415 influence at least 2 traits with $r_W < 0.2$. To investigate how often pleiotropy is not
416 predicted by the degree to which morphological features correlate in the absence of
417 genetic variation, in the next section we compare trait correlations present across clones
418 (r_W) to those present between genetically diverse strains (r_B).

419

420 ***Many traits are more strongly correlated across strains than they are across clones***

421 When genetic changes that perturb one trait have collateral effects on another, we
422 expect the way traits correlate across genetically diverse strains to reflect trait
423 correlations across clones (*i.e.* $r_B = r_W$). When this condition is met, pleiotropy can be
424 viewed as an expected consequence of inherent relationships between traits, *i.e.* vertical
425 pleiotropy. On the other hand, if a QTL influences two traits that do not correlate across
426 clones, it may cause these traits to correlate across strains in which this QTL is
427 segregating. In this case, we expect r_B will be greater than r_W , suggesting horizontal
428 pleiotropy.

429 After correcting for multiple hypothesis testing, r_B significantly exceeds r_W in
430 24% of all trait pairs, and 41% of pairs in which at least one pleiotropic QTL influences
431 both traits (**Fig 3**; left panel; 41% of points are above the envelope, which represents a
432 Bonferroni corrected significance threshold of $p < 0.01$). In the majority of cases in which
433 r_B significantly differs from r_W , r_B is greater than r_W (**Fig 3**; left panel; 83% of points
434 outside the envelope are above it). The magnitude of the increase in r_B vs. r_W tends to
435 scale with the number of pleiotropic QTL that jointly influence both traits in a pair (**Fig**
436 **3**; left panel; colors get warmer farther above the envelope). These observations are
437 consistent with the hypothesis that QTL acting via horizontal pleiotropy increase r_B
438 relative to r_W .

439 However, horizontal pleiotropy is not the only reason traits may correlate
440 differently across strains versus across clones. We find significant deviations in r_B
441 relative to r_W in 14% of pairs for which no pleiotropic QTL influence both traits, (**Fig 3**;
442 right panel). This observation may suggest the presence of pleiotropic genetic variants
443 that we did not have statistical power to detect with an FDR of 5% in our QTL screen.
444 But an alternate explanation for the observed increases in r_B over r_W is that perhaps we
445 sometimes underestimate r_W .

446 One reason r_W could be underestimated is that single-cell measurements are
447 noisier than group-level averages. To test this possibility, we randomly assigned
448 individual cells to groups (pseudo-strains) having the same number of cells as the actual
449 strains, and found that in these permuted data, r_B and r_W never significantly differ (**Fig 3**;
450 insets). Because detection of r_W was not underpowered relative to r_B , we conclude that

451 measurement noise does not meaningfully obscure r_W . Another reason r_W could be
452 underestimated is if trait correlations across strains are more linear than those across
453 clones. To test this possibility, for every pair of traits we transformed the single-cell trait
454 measurements using a nonparametric model that finds their maximal correlation [70].
455 This transformation abrogated significant differences in r_B relative to r_W for fewer than
456 5% of affected trait pairs. Another reason r_W might be less than r_B is if there tends to be
457 less phenotypic variation within strains than between strains. Contrary to this prediction,
458 every morphological trait we surveyed varies more within strains than between strains. A
459 final reason r_W could be poorly estimated is if non-genetic heterogeneity across different
460 subpopulations within clonal populations causes variation in r_W . Therefore, next we
461 investigated whether the relationship between single-cell features varies for clonal cells
462 in different stages of the cell-division cycle.

463

464 *Inferring a cell's progress through division from fixed cell images*

465 Pairs of traits for which r_B is strong whereas r_W is not should reflect horizontal
466 pleiotropy, but a closer examination of some of these pairs revealed traits that should
467 correlate due to simple geometric constraints. For example, cell size and the width of the
468 bud neck should correlate due to the constraint that, even at its maximum, bud neck width
469 cannot be larger than the diameter of the cell. When measured in small-budded cells,
470 these two traits are correlated across yeast strains ($r_B = 0.40$) but are significantly less
471 correlated across clones ($r_W = 0.15$). Given the simple geometric constraint coupling the
472 width of the bud neck to the cell's size, why is there a discrepancy between r_B and r_W ?
473 We reasoned that this discrepancy exists because the correlation between cell size and
474 neck width is disrupted during particular moments of cell division; e.g. the width of the
475 bud neck starts small even for large cells (**Fig 4A**; cell micrographs outlined in blue show
476 two cells in the progress of budding). If the relationship between morphological features
477 varies during cell division, r_W may represent a poor summary statistic.

478 How often does the relationship between morphological traits change during cell
479 division? Our single cell measurements are primed to address this question: we fixed
480 cells during exponential growth and imaged hundreds of thousands of single cells,
481 thereby capturing the full spectrum of morphologies as cells divide. A remaining
482 challenge is sorting these images according to progress through cell division, and then re-
483 measuring the correlation between morphological features within narrow windows along
484 that progression.

485 We performed this sorting using the Wishbone algorithm [71]. This algorithm
486 extracts developmental trajectories from high-dimensional phenotype data (typically
487 single-cell transcriptome data). We applied Wishbone separately to cells belonging to
488 each of the three cell types defined by morphometric analysis (unbudded, small-budded,
489 and large-budded cells). The trends describing how morphological features vary across
490 Wishbone-defined cell-division trajectories are consistent with previous observations of
491 how morphology changes in as yeast cells divide [72,73] (**Fig 4A**; line plots). For
492 example, Wishbone sorts fixed-cell images in such a way that cell area increases
493 throughout the course of cell division (**Fig4A**; upper left panel), and nuclear elongation
494 occurs just before nuclear division (**Fig4A**; lower left panel). These trajectories also
495 match our own observations of how morphological features change as live cells divide,
496 which we tracked by imaging at 1-minute intervals one of the 374 progeny strains that we

497 had engineered to express a fluorescently tagged nuclear protein (HTB2-GFP) (**Fig 4A**;
498 micrographs). We chose this particular strain because it does not deviate from the average
499 morphology of all 374 recombinants by more than one standard deviation for any of the
500 phenotypes we measure.

501 To further validate Wishbone's performance, we asked whether it could
502 reconstruct the time series of live-cell images from the HTB2-GFP strain. We obtained
503 time series for 78 single dividing cells, each imaged over at least 20 timepoints.
504 Quantifying morphological phenotypes from live-cell images in a high-throughput
505 fashion proved difficult because the morphometric software was optimized for fixed-cell
506 images and as cells grow and bud, the cells and their nuclei can move out of the focal
507 plane. Also, although we used short exposure times when imaging GFP fluorescence,
508 there are concerns about photo-toxicity and associated growth and morphology defects
509 [74]. For these reasons, we expect Wishbone to perform better on fixed-cell images than
510 on time series of live cell images. Still, Wishbone's cell-division trajectories recapitulate
511 the time course. When we align time series data across live cells by centering on each
512 cell's average predicted progress through division, Spearman's r is 0.65, 0.91, and 0.77
513 for time series corresponding to each of the three cell types (**Fig 4B**; see **Fig S5** for
514 recapitulation of 78 individual time series). These correlations are substantially higher
515 than those obtained by repeating the merging procedure after randomly permuting each
516 time series (corresponding Spearman's r of 0.42, 0.43, and 0.56). These observations
517 suggest that Wishbone is effective at properly assigning single-cell images to their
518 position in the cell cycle.

519

520 *Cell cycle state can influence the relationship between morphological features*

521 To identify cases where significant differences in r_B vs. r_W might result because
522 r_W is sensitive to cell-cycle state, we first assigned each imaged yeast cell from the QTL-
523 mapping population to one of 16 equal-sized bins based on Wishbone's estimation of
524 how far that cell had progressed through division. Because we did this separately for each
525 of the previously defined cell stages (unbudded, small-budded, and large-budded), this
526 additional binning finely partitions cell division into 48 (16 x 3) stages. To hold genotype
527 representation constant across each of the 48 bins, we performed binning separately for
528 each of the 374 mapping-family strains, then merged like bins across strains. We then
529 performed correlation partitioning on each bin separately.

530 Binning cells by cell-cycle state typically decreased the amount of phenotypic
531 variation per bin, which we expect in turn to obscure the correlation between traits.
532 Consider an extreme example: if there is no phenotypic variation remaining for a given
533 trait, it cannot covary with any other traits. Indeed, for most pairs of traits, the binning
534 procedure either decreases r_W or does not have a dramatic effect on it; decreases in r_W are
535 especially evident for trait pairs where variation of at least one of the traits shows a
536 relatively large decrease upon binning (**Fig 4C**). However, for some pairs of traits,
537 despite the decrease in phenotypic variation for at least one trait, the correlation between
538 traits improves upon binning. For example, binning by cell division increases the
539 correlation between cell size and the width of the bud neck (**Fig 4D**; leftmost plot) such
540 that it approaches r_B . This increased correlation is consistent with our hypothesis that the
541 process of cell division was obscuring the dependency of bud neck width on cell size.
542 Examining more pairs of traits for which binning tends to increase r_W (**Fig 4C**; red,
543 orange, and yellow points) reveals additional cases where the process of cell division

544 decouples traits that are otherwise correlated, and where binning reveals the underlying
545 correlation (**Fig 4D**; leftmost three plots).

546 Despite the evidence that cell asynchrony alters some trait correlations, many
547 cases remain where heterogeneity in cell-cycle state does not explain the observed
548 discrepancy between r_W and r_B (**Fig 4D**; rightmost three plots). We previously
549 demonstrated that r_B significantly exceeds r_W in 24% of all trait pairs (1389/5645) (**Fig**
550 **3**). For almost half of these pairs (689 pairs), binning by cell division does not resolve the
551 discrepancy between r_B and r_W to any extent; in other words, r_W does not increase in any
552 of the 16 bins. For an additional 193 pairs, binning by cell division resolves the
553 discrepancy by at most 5% in any bin. These results imply that cell-cycle heterogeneity
554 does not cause the discrepancy between r_W and r_B in the majority of cases, and that
555 elevation of r_B over r_W is best explained by QTL demonstrating horizontal pleiotropy.

556

557 ***Many QTL demonstrate horizontal pleiotropy***

558 To test horizontal pleiotropy further, we focused on the 24 QTL each found to
559 influence at least 2 traits with $r_W < 0.2$ (pleiotropic QTL not included in **Fig 2B**). To test
560 whether these pleiotropic QTL cause increases in r_B relative to r_W , we divided our yeast
561 strains into sets in which a given QTL is not segregating, then re-measured the difference
562 between r_B and r_W . More specifically, for each QTL, we split the 374 phenotyped yeast
563 strains into two groups based on whether they inherited the wine or the oak parent's allele
564 at the genotyped marker closest to the estimated QTL location. Then we repeated
565 correlation partitioning on each subset of strains and compared the results to those
566 obtained from the complete set. For each QTL, we focused on trait pairs in which: (1)
567 both traits are affected by this QTL, and (2) r_B is significantly greater than r_W . Across all
568 such pairs, median r_B tends to decrease upon eliminating allelic variation at the marker
569 nearest the QTL (**Fig 5A**). No similar reduction in r_B is observed when we focus on pairs
570 of traits that are not affected by each QTL (**Fig 5A**) and no similar reduction is observed
571 in r_W (median reduction in r_W is 0.0001).

572 There appear to be two ways in which a QTL may affect r_B . In some cases,
573 eliminating genetic variation at the marker nearest a QTL decreases r_B in both resulting
574 subpopulations. Such cases are consistent with a straightforward scenario in which
575 horizontal pleiotropy results when a QTL that influences two or more traits (that are
576 otherwise weakly correlated) is segregating in a population (**Fig 5B**; top row). In other
577 cases, eliminating allelic variation at a QTL site decreases r_B in only one of the two
578 resulting subpopulations (*i.e.* the subpopulation possessing either the oak or the wine
579 allele). This observation demonstrates that horizontal pleiotropy can emerge by virtue of
580 a QTL allele strengthening a correlation between two traits so that genetic variation
581 affecting one trait is more likely to affect the other when that allele is present [76,77] (**Fig**
582 **5B**; bottom row).

583 How many cases where r_B significantly exceeds r_W can be explained, to some
584 extent, by horizontal pleiotropy (*i.e.* a QTL increasing the between-genotype
585 correlation)? For every trait pair where r_B significantly exceeds r_W and at least one QTL
586 influences both traits in the pair (1153 pairs total), eliminating allelic variation at the
587 marker nearest at least one of the shared QTL causes r_B to decrease in one or both of the
588 resulting subpopulations (**Fig 5C**: solid black line in rightmost plot). About 60% of these
589 decreases affect both subpopulations (*e.g.* **Fig 5B**; top row) and 40% affect only one

590 subpopulation (e.g. **Fig 5B**; bottom row). These decreases in r_B appear to resolve the
591 discrepancies in r_B vs. r_W more often and to a greater extent than does accounting for
592 cell-cycle heterogeneity (**Fig 5C**; leftmost plot). Some QTL have larger impacts on r_B
593 than do others (**Fig 5C**). Eliminating allelic variation near a QTL on chromosome 13
594 decreases r_B in the largest number of traits pairs (681). Subtracting the influence of a
595 QTL on chromosome 15 decreases r_B to the greatest extent; the average decrease across
596 357 affected trait pairs is 0.07. Together these observations suggest: (1) many QTL
597 demonstrate horizontal pleiotropy (**Fig 5A**), (2) there are at least two ways for horizontal
598 pleiotropy to emerge (**Fig 5B**), and (3) horizontal pleiotropy is a major factor driving
599 increases in r_B over r_W in this study (**Fig 5C**).

600

601 *Spontaneous mutations alter the relationships between morphological features*

602 Our finding that some QTL alleles appear to strengthen correlations between
603 otherwise weakly correlated traits (**Fig 5B**; lower panel) lends credence to the idea that
604 the relationships between phenotypes, and thus the extent of phenotypic modularity (or
605 integration), are mutable traits [78]. This finding has implications for evolutionary
606 medicine, in particular evolutionary traps, e.g. strategies to contain microbial populations
607 by encouraging them to evolve resistance to one treatment so that they become
608 susceptible to another [39-41]. These traps will fail if targeted correlations can be broken
609 by mutations. To test whether spontaneous mutations can alter trait correlations, we
610 analyzed the cell-morphology phenotypes of a collection of yeast mutation-accumulation
611 (MA) lines [54]. These MA lines were derived from repeated passaging through
612 bottlenecks, which dramatically reduced the efficiency of selection and thereby allowed
613 retention of the natural spectrum of mutations irrespective of effect on fitness [55]. We
614 previously imaged these lines in high throughput (>1000 clonal cells imaged per each of
615 94 lines) [50].

616 Because MA lines contain private mutations unique to each strain, they are not
617 amenable to QTL mapping and between-strain trait correlations have less meaning.
618 Instead, we focused on within-strain correlations, which we expected to be consistent
619 across strains because of the limited number of mutations distinguishing the strains (an
620 average of 4 single-nucleotide mutations per line [55]), except if a rare mutation does
621 indeed alter the correlation. To determine if such correlation-altering mutations exist, we
622 calculated within-strain correlations for each strain separately and asked, for each trait
623 pair, whether any strains had extreme correlations relative to the other strains. For most
624 trait pairs, the MA lines trait correlations did not vary much from each other or from that
625 of the ancestor strain (**Fig 6**). However, in several instances, we observed a trait-pair
626 correlation dramatically outside the range of the other trait pairs and more than four
627 standard deviations from the mean (**Fig 6A**). Some mutations appear to influence many
628 trait-trait relationships (mutations found in blue- and purple-colored strains in **Fig 6B &**
629 **C**), whereas others influence fewer (mutations found in magenta-colored strain in **Fig**
630 **6C**).

631 Given that in this small sampling of spontaneous mutations, we found several that
632 appear to alter the relationship between morphological features, we think such mutations
633 are common enough to merit further consideration in evolutionary models. The mutations
634 in the outlier lines provide candidate correlation-altering mutations for future mechanistic
635 studies as well.

636

637 **Discussion:**

638 Although evolutionary biologists and medical geneticists alike appreciate that
639 organismal traits can rarely be understood in isolation, the extent and implications of
640 pleiotropy have remained difficult to assess. One approach to measuring pleiotropy has
641 been to count phenotypes influenced by individual genetic loci [17,33,34]. For example,
642 the median number of skeletal traits affected per QTL in a mouse cross was six (out of 70
643 traits measured); this small median fraction of traits suggests that variation in skeletal
644 morphology is modular [16,30]. Of course, for a count of traits to be meaningful the full
645 trait list must be comprehensive, and correlations between traits must be properly
646 accounted for [17,33,34]. We aimed for comprehensiveness in a very similar way to the
647 studies of mouse skeletal traits, by systematic phenotyping of a large number of
648 morphological traits. However, we addressed the need for a principled approach to
649 separating inherent trait correlations from those induced by genetic differences in a new
650 way: by extending the analysis to include within-genotype correlations and thereby
651 enabling an operational definition of the distinction between vertical and horizontal
652 pleiotropy.

653 Our comprehensive analysis of how thousands of trait pairs co-vary within and
654 between mapping strains yields an unprecedentedly quantitative and nuanced view of
655 pleiotropy. We found support for modularity, not only in the striking correspondence
656 between our median number of traits affected per QTL (six out of 167) and that found for
657 mouse skeletal traits [16,30], but also in the way that within-genotype correlations
658 grouped traits into relatively isolated clusters (**Fig 2**). We also found ample evidence of
659 horizontal pleiotropy layered on top of that modularity, with many cases of between-
660 genotype trait correlations that exceeded within-genotype correlations (**Fig 3**). Our results
661 do not speak directly to whether modularity results from selection against pleiotropy in
662 nature, because we sampled only two natural genetic backgrounds (wine and oak).
663 However, future work comparing MA lines to a larger collection of natural isolates might
664 help answer questions about the extent to which selection purges pleiotropic mutations.

665 Our partitioning of between-strain (genetic) and within-strain (environmental)
666 correlations relates to another approach to understanding trait interdependencies, the
667 estimation of the so-called **G** matrix. This genetic variance-covariance matrix
668 summarizes the joint pattern of heritable variation in a population of the traits that
669 compose its rows and columns, and is central to understanding how trait correlations
670 constrain evolution. The **G** matrix arises in the multivariate breeder's equation, which
671 describes the responses to selection of correlated traits [79]. If breeding is the goal, the
672 distinction between vertical and horizontal pleiotropy is not so important, because both
673 can impede selection. Indeed, any philosophical concern about what constitutes a
674 biologically meaningful trait is irrelevant to the breeder, who actually cares about
675 particular traits (*e.g.*, milk yield and fat content).

676 **G** matrices are not only relevant to breeders, but to evolutionary biologists as
677 well, and it is worthwhile to place our results into this context. A major evolutionary
678 question in the **G**-matrix literature is whether the **G** matrix itself can evolve. In other
679 words, do short-term responses to selection (as captured in the breeder's equation) predict
680 long-term responses or do constraints shift through time, perhaps in a way that facilitates
681 (or is part of) adaptation [80]? Our results with MA lines add to evidence that the **G**
682 matrix readily changes [81], in that individual mutations have major effects on particular

683 trait correlations (*e.g.* **Fig 6A**). Our QTL-mapping results also support this view, in that
684 some cases of horizontal pleiotropy appear to be caused by alleles that alter trait
685 correlations (*e.g.* **Fig 5B**; bottom panel).

686 Another prominent question in the **G**-matrix literature is the extent to which the **P**
687 matrix, which includes all sources of phenotypic variation and covariation, predicts the **G**
688 matrix, which only includes additive genetic effects (*i.e.*, those that respond to selection).
689 If **P** predicts **G** well, as proposed by Cheverud [82], then inference of selection responses
690 from patterns of trait covariation in a population would suffice when genetic analysis
691 would be difficult or costly. Our results do not speak directly to this question, because we
692 did not estimate **G** itself and instead estimated genetic correlations that include non-
693 additive effects. However, our results are informative from another angle, which is the
694 comparison of genetic and environmental correlations. As we showed (**Fig 3**), although
695 there are cases in which the environmental and genetic correlations have different signs,
696 the environmental correlations do tend to match the signs of the genetic correlations and
697 predict their magnitudes to some extent as well, consistent with similarity between **P** and
698 **G**. Future experiments using clones embedded in a more complicated crossing scheme
699 could properly partition **P** into **G**, **E**, and the non-additive genetic components, to address
700 Cheverud's conjecture [82] more directly. There are only a few reports of comparisons of
701 **E** matrices [83], but we encourage increased attention to the **E** matrix to understand
702 inherent trait correlations and to contextualize **G** in a way that diminishes concerns about
703 which traits have been granted status as its rows and columns.

704 A major conclusion of our work is that context is crucial. We have shown that
705 trait correlations change through the cell-division cycle and in different genetic
706 backgrounds. It is likely that macroenvironmental differences alter trait correlations as
707 well [84]. These results support the idea that predicting the mapping from genotype to
708 phenotype requires a paradigm shift [85], away from merely mapping the relationships
709 between traits and toward unfurling the range of contexts across which those
710 relationships persist. Future work in this direction will not only advance understanding of
711 the evolution of complex traits, but will have practical benefits. For example, our
712 approach demonstrates a potentially fruitful way to consider the design of evolutionary
713 traps: using within-genotype correlations to identify particularly immutable inherent
714 correlations between traits.

715

716 **Acknowledgments:**

717 We are grateful to Dmitri Petrov and Grant Kinsler for helpful discussions about
718 pleiotropy and comments on an earlier version of this manuscript. We also thank Barak
719 Cohen and David Hall for providing strains used in this study. This work was supported
720 by National Institutes of Health grant R35GM118170 (to MLS), National Institutes of
721 Health fellowship F32GM103166 (to KGS), a New York University Graduate School of
722 Arts and Science Dean's Dissertation Fellowship (to SL), and National Institutes of
723 Health grant R35GM119744 (to ABP). The funders had no role in study design, data
724 collection and analysis, decision to publish, or preparation of the manuscript.

725

726 **Materials and Methods:**

727 *Measuring the morphology of single yeast cells*

728 Recombinant yeast strains were generated and genotyped at 225 markers in a previous
729 study [53,59]; each strain is a homothallic diploid. We prepared yeast cells from these
730 strains for microscopy using published methods [49-51,86]. Briefly, yeast strains were
731 grown in minimal media with 0.08% glucose in 96-well plates [87], harvested during
732 exponential phase, fixed in 4% paraformaldehyde, stained for cell-surface manno-protein
733 (with FITC-concanavalin A) and nuclear DNA (with DAPI), sonicated, mounted on 96-
734 well glass-bottom microscopy plates, and imaged with a Nikon Eclipse TE-2000E
735 epifluorescence automated microscope using a 40× objective and appropriate
736 fluorescence filters. Three biological replicate experiments were performed, typically
737 yielding a total of between 500 to 1,000 imaged cells per strain (**Fig S2**).

738

739 *Statistical analysis and processing of cell image data*

740 Cell image processing was performed similarly to previous studies [49-51,86]. Imaged
741 cells were analyzed for quantitative morphological traits using the CalMorph software
742 package [52], which reports on hundreds of morphological features that are each specific
743 to one of three cell types: unbudded, small-budded, and large-budded cells. We excluded
744 phenotypes for which >10% of cells had missing values, leaving 167 morphological
745 features. Any cell that was not scored for all features pertaining to its type was
746 eliminated. Each morphological trait was transformed via a Box-Cox transformation of
747 the raw data with the value of lambda that makes the residuals of a linear regression of
748 phenotype on strain most normal using the EnvStats package in R [88]. Internal controls
749 (several wells representing the wine and oak parents) were present on every 96-well plate
750 and were used to correct for effects on phenotypic variation that resulted from differences
751 among replicate experiments, such as differences in the brightness of the cell stain. We
752 calculated the mid-parent value for each phenotype on every plate, then calculated the
753 average mid-parent value across all plates. For each phenotype, we found the difference
754 between the plate-specific mid-parent value and the average mid-parent value across all
755 plates. Then we subtracted this difference from each plate for the corresponding
756 phenotype. After correction, any cell with a morphological feature that deviated from the
757 average by more than 5 standard deviations was then eliminated, as investigation of such
758 cells typically revealed these were CalMorph miscalls or cellular debris.

759

760 *QTL mapping*

761 QTL interval mapping was performed similarly to previous studies [62] using the R/qtl
762 package [63]. We performed a QTL scan using the function “scanone”, which finds at
763 most one QTL per chromosome. Yeast strains, which are homozygous diploids, were
764 modeled as haploids and QTL models were fit using Haley-Knott regression. As in
765 previous work [62], when comparing QTL across traits, QTL within 30 cM on the same
766 chromosome were counted as the same QTL. In some cases, we detected a QTL in
767 between two others on the same chromosome and within 30 cM of both. In these cases,
768 we made decisions about the total number of unique QTL present by using our best
769 judgement and considering factors such as the proximity between QTL. A summary of all
770 significant QTL effects, including their chromosomal locations in cM and which QTL on
771 the same chromosome we considered unique, is provided in **Table S1** (also see **Fig 1A**).
772 QTL effects were counted as significant when they were stronger than any QTL effect

773 detected in 100 randomly permuted datasets, allowing for 5% false positives.
774 Permutations were performed separately for each trait.

775

776 *Candidate gene swaps*

777 All yeast transformations were performed using the lithium acetate [89] and *delitto*
778 *perfetto* [64] methods. For each candidate gene, the gene was first deleted from haploid
779 variants of both the wine and oak parental strains and replaced with a selectable marker,
780 the yeast gene encoding orotidine-5'-phosphate decarboxylase (*URA3*). Gene knockouts
781 were confirmed by growth on plates lacking uracil and DNA sequencing of the affected
782 region. Next, the *URA3* selectable marker was replaced with the other parent's version of
783 the candidate gene. These candidate gene 'swaps' were selected by growth on 5-
784 Fluoroorotic acid and confirmed by sequencing of the affected region. For each candidate
785 gene, we swapped a region containing the coding sequence plus 5 – 750 bp up and
786 downstream. We used the following regions of homology to define the boundaries of
787 each swapped segment:

788

789 ~300bp upstream of *PXLI*: TTATAATTGTGGTTTAGCGTTTCATAGTCGC

790 ~300bp downstream of *PXLI*: CCTTATTCTCTATTCTTAGGCTCCTGTTCC

791 ~5bp upstream of *HOF1*: GAAAGAATGAGCTACAGTTATGAAGCTTG

792 ~ 300bp downstream of *HOF1*: GTATTTCGTAACAAGTGACTCTAATGATAT

793 ~ 750bp upstream of *RASI*: CGACTAAAGGAATTATAACCATCATGCATC

794 ~ 300bp downstream of *RASI*: GCATTTCTAAAAACAGAGCTTTTGCCG

795

796 These regions of homology were chosen by searching for regions of higher GC content
797 nearby the start and end of each gene's coding sequence. In addition, we attempted to
798 swap the wine and oak parents' versions of the *GPAL* gene on chromosome 8. Despite
799 trying various regions of homology, we could not successfully replace *GPAL* with the
800 *URA3* selectable marker in the oak parent. *GPAL* is known to be essential in some genetic
801 backgrounds [90].

802

803 Though the recombinant strains we studied are homothallic diploids, the strains in **Fig 1B**
804 (both the parental strains and the strains possessing the gene swaps) are haploid. Because
805 the analyses in **Fig 1B** compare pairs of strains (*e.g.* the oak haploid parent to the wine
806 haploid parent, or the wine haploid parent to the wine haploid parent possessing the oak
807 allele of *PXLI*), we only considered experiments where both strains in the pair were
808 imaged in the same replicate experiment. To account for differences among replicate
809 experiments, for each phenotype, we subtracted the value in one strain from the value in
810 the other to calculate the phenotypic difference between strains in that replicate
811 experiment; the reported value is the average of these differences across replicate
812 experiments (**Table S2, Fig 1B**).

813

814 *Calculation of correlation coefficients*

815 We used WABA II as implemented in the multilevel package in R [69] to
816 calculate cell-level (r_W) and strain-level (r_B) Pearson correlation coefficients for each pair
817 of traits. We used an r-to-z transformation to determine whether differences in r_B vs. r_W
818 are significant at a Bonferroni corrected p-value of 0.01 (this is a z-score cutoff of 4.63,

819 given 5645 pairs of traits were tested). To assess whether correlations across single cells
820 generally result in different values than correlations across group-level averages, we
821 assigned yeast cells to groups (pseudo-strains) randomly, maintaining the same number
822 of cells per strain as in the actual data. To assess whether results would differ if we
823 allowed for non-linear correlations, we transformed the single-cell data using a
824 nonparametric model that finds the fixed point of maximal correlation, implemented in
825 the R package *acepack* [70]. To assess whether results from WABA differed from those
826 obtained using a standard quantitative genetics model (**Fig S3**), we implemented the latter
827 using the *nlme* package in R [91] to specify a mixed-effects model with cells nested
828 within strains. We specified a covariance structure that allows covariance between two
829 traits but no covariance between cells or between strains. We used this model to calculate
830 the environmental and genetic correlations for 350 pairs of randomly chosen traits.

831

832 *Live imaging single cells as they divide*

833 For live imaging the morphology of dividing yeast cells, we chose one of the
834 recombinant yeast strains, F2_292. This strain was chosen because it does not deviate
835 from the average morphology of all 374 recombinants by more than one standard
836 deviation for any of the phenotypes we measured. F2_292 was transformed to express a
837 fusion protein of GFP and a nuclear protein (histone H2B encoded by *HTB2*). Two
838 independent transformants were imaged in the GFP channel (for nuclei) and in brightfield
839 (for cell outlines). We prepared live cells for imaging following published methods
840 [87,92,93], in a similar way to that described above, except cells were neither fixed nor
841 stained. Cells were taken during mid-log phase growth, seeded in 96-well glass bottom
842 microscopy plates containing minimal media with 0.08% glucose, and imaged over a
843 period of 3 hours. In each of four replicate experiments, cells were imaged either every
844 minute, every 90 seconds, or every 2 minutes. We used short exposure times (afforded by
845 the highly abundant HTB2-GFP) and took only a single image per well per timepoint to
846 reduce photo-toxicity. We processed images with CalMorph then matched cells across
847 timepoints by their centroid locations in the imaging fields. Overall we obtained time
848 series for 78 cells that each: (1) were longer than 20 timepoints, (2) contained no gaps
849 where the cell was not phenotyped for many consecutive timepoints, and (3) contained no
850 images that appeared to be very out of focus potentially resulting in misestimation of
851 phenotype values. Because CalMorph divides cells into unbudded, small-budded and
852 large-budded stages, these 78 time series are also divided this way (11, 23, and 44 cells,
853 respectively).

854

855 We used the Wishbone algorithm implemented in python [71] to estimate progression
856 through the cell-division cycle. Wishbone recapitulates each of these 78 time series (**Fig**
857 **S5**) with Spearman correlations between the actual and inferred image orders that average
858 0.42, 0.85, 0.40 across all unbudded, small-budded or large-budded series, respectively.
859 The lower correlations between Wishbone's predicted progress through division and time
860 for the unbudded and large-budded cells may result because each time series captured
861 only a part of the cell-division cycle and, during some stretches in the cycle, there are
862 fewer morphological changes taking place. To estimate Wishbone's accuracy across a
863 longer stretch of time, we merged the Wishbone predictions within the classes of
864 unbudded, small-budded or large-budded cell time series. To do so, we had to contend

865 with the fact that the first timepoint for each imaged cell often represents a different
866 moment in division. For example, some time series for unbudded cells start from an
867 image that is already far along the division process (**Fig S5**; values close to 1 on the
868 vertical axis) while others start from a cell image that has just begun its division cycle
869 (**Fig S5**; values close to zero on the vertical axis). Therefore, we aligned the time series
870 by subtracting from each the difference between Wishbone's estimate of the average
871 percent progress through division and the average time elapsed.

872

873 Note that, because this merging procedure utilized information from Wishbone, it
874 imposes a correlation between time and Wishbone's estimated progress through division.
875 To reduce the impact of this induced correlation, we eliminated the cell images in the
876 middle of each time series, which represent the images that are most affected by this
877 induced correlation. Eliminating 25% or 50% of cell images in this way reduced the
878 correlations by at most 0.05, suggesting these correlations are not driven by our merging
879 procedure.

880

881 *Assigning cells to a bin based on progression through cell division*

882 We used Wishbone to estimate how far each fixed-cell image had progressed through cell
883 division. Wishbone software requires input about which "start" cell has features
884 resembling those present at the start of the cell cycle. To identify such features, we used
885 the data from the live-imaged cell time series. We plotted how single-cell features change
886 over the course of live imaging, and chose several features that correlate best with
887 progress through cell division (*e.g.* cell size, bud size, location of the nucleus).

888

889 Using Wishbone's estimation of how far each fixed cell had progressed through division,
890 we assigned each cell to one of 16 equal-sized bins. We did this separately for each of the
891 374 yeast strains, then merged like bins across strains, such that genetic diversity was
892 constant across each of the final 16 bins. We obtained very similar results to those
893 reported in **Figs 4C, 4D, and 5C** when we used 8 instead of 16 bins. The names of the
894 traits plotted in **Fig 4** represent succinct summaries of single-cell morphologies
895 quantified using CalMorph [52]. For fuller descriptions of these traits, see the following
896 trait designations in the CalMorph software manual: **Fig 4A** upper left: C11.1 in
897 unbudded cells, C101 in budded cells; **Fig 4A** lower left: D184 in small-budded cells,
898 D182 in unbudded and large-budded cells; **Fig 4A** upper right: C12.2; **Fig 4A** lower
899 right: D116; **Fig 4C** upper left: C101 and C109 in small-budded cells; **Fig 4C** upper
900 middle: C11.2 and D132 in small-budded cells; **Fig 4C** upper right: C105 and C113 in
901 small-budded cells; **Fig 4C** lower left: C114 and D145 in large-budded cells; **Fig 4C**
902 lower middle: C109 and C126 in large-budded cells; **Fig 4C** lower right: D14.2 and D169
903 in large-budded cells.

904

905 *Eliminating genetic variation at the marker nearest a QTL*

906 For each of the 24 QTL suspected of horizontal pleiotropy (*i.e.* pleiotropic QTL not in
907 **Fig 2B**), we divided the 374 phenotyped yeast strains into two groups based on whether
908 they inherited the wine or the oak parent's allele at the genotyped marker closest to the
909 QTL. We then performed correlation partitioning separately for each group of strains.
910 The names of the traits plotted in **Fig 5B** represent succinct summaries of single-cell

911 morphologies quantified using CalMorph. For fuller descriptions of these traits, see the
912 following trait designations in the CalMorph software manual: upper: D128 and C114 in
913 large-budded cells; lower: D197 and D17.1 in large-budded cells.

914

915 *Quantifying trait correlations within each MA line*

916 We used MA line data from our previous study [50]. Fewer traits were analyzed in that
917 study than in the current study, such that there were only 3731 pairs of traits to survey, as
918 opposed to 5645 in the QTL-mapping family. We calculated Pearson correlations
919 between every pair of traits, separately within each MA line. The names of the traits
920 plotted in **Fig 6A** represent succinct summaries of single-cell morphologies quantified
921 using CalMorph. For fuller descriptions of these traits, see the following trait
922 designations in the CalMorph software manual: upper left: D185 and D186 in large-
923 budded cells; upper right: C102 and D132 in small-budded cells; lower left: C108 and
924 D167 in large-budded cells; lower right: D135 and D169 in large-budded cells.

925

926 **References:**

927

- 928 1. Plate L. Genetics and evolution. Fischer J, editor. Fest schrift zum sechzigsten
929 Geburtstag Richard Hertwigs; 1910. pp. 536–610.
- 930 2. Stearns FW. One Hundred Years of Pleiotropy: A Retrospective. *Genetics*.
931 *Genetics*; 2010;186: 767–773. doi:10.1534/genetics.110.122549
- 932 3. Simons YB, Bullaughey K, Hudson RR, Sella G. A population genetic
933 interpretation of GWAS findings for human quantitative traits. Gibson G, editor.
934 *PLoS Biol*. 2018;16: e2002985. doi:10.1371/journal.pbio.2002985
- 935 4. Tyler AL, Asselbergs FW, Williams SM, Moore JH. Shadows of complexity: what
936 biological networks reveal about epistasis and pleiotropy. *Bioessays*. WILEY-
937 VCH Verlag; 2009;31: 220–227. doi:10.1002/bies.200800022
- 938 5. Visscher PM, Wray NR, Zhang Q, Sklar P, McCarthy MI, Brown MA, et al. 10
939 Years of GWAS Discovery: Biology, Function, and Translation. *Am J Hum Genet*.
940 2017;101: 5–22. doi:10.1016/j.ajhg.2017.06.005
- 941 6. Visscher PM, Yang J. A plethora of pleiotropy across complex traits. *Nat Genet*.
942 2016;48: 707–708. doi:10.1038/ng.3604
- 943 7. Chesmore K, Bartlett J, Williams SM. The ubiquity of pleiotropy in human
944 disease. *Hum Genet*. 137: 39–44.
- 945 8. Sivakumaran S, Agakov F, Theodoratou E, Prendergast JG, Zgaga L, Manolio T,
946 et al. Abundant pleiotropy in human complex diseases and traits. *Am J Hum*
947 *Genet*. Elsevier; 2011;89: 607–618. doi:10.1016/j.ajhg.2011.10.004

- 948 9. White JK, Gerdin A-K, Karp NA, Ryder E, Buljan M, Bussell JN, et al. Genome-
949 wide generation and systematic phenotyping of knockout mice reveals new roles
950 for many genes. *Cell*. Elsevier; 2013;154: 452–464. doi:10.1016/j.cell.2013.06.022
- 951 10. Wang Z, Liao B-Y, Zhang J. Genomic patterns of pleiotropy and the evolution of
952 complexity. *Proc Natl Acad Sci USA*. National Acad Sciences; 2010;107: 18034–
953 18039. doi:10.1073/pnas.1004666107
- 954 11. Housman G, Byler S, Heerboth S, Lapinska K, Longacre M, Snyder N, et al. Drug
955 resistance in cancer: an overview. *Cancers (Basel)*. Multidisciplinary Digital
956 Publishing Institute; 2014;6: 1769–1792. doi:10.3390/cancers6031769
- 957 12. Rockman MV. The QTN program and the alleles that matter for evolution: all
958 that's gold does not glitter. *Evolution*. 2012;66: 1–17. doi:10.1111/j.1558-
959 5646.2011.01486.x
- 960 13. Boyle EA, Li YI, Pritchard JK. An Expanded View of Complex Traits: From
961 Polygenic to Omnigenic. *Cell*. 2017;169: 1177–1186.
- 962 14. Fisher RA. *The Genetical Theory of Selection*. Clarendon. 1930.
- 963 15. Allen Orr H. Adaptation and the cost of complexity. *Evolution*. 2000;54: 13.
964 doi:10.1554/0014-3820(2000)054[0013:AATCOC]2.0.CO;2
- 965 16. Wagner GP, Kenney-Hunt JP, Pavlicev M, Peck JR, Waxman D, Cheverud JM.
966 Pleiotropic scaling of gene effects and the 'cost of complexity'. *Nature*. Nature
967 Publishing Group; 2008;452: 470–472. doi:10.1038/nature06756
- 968 17. Wagner GP, Zhang J. The pleiotropic structure of the genotype–phenotype map:
969 the evolvability of complex organisms. *Nat Rev Genet*. Nature Publishing Group;
970 2011;12: 204–213. doi:10.1038/nrg2949
- 971 18. McGee LW, Sackman AM, Morrison AJ, Pierce J, Anisman J, Rokyta DR.
972 Synergistic Pleiotropy Overrides the Costs of Complexity in Viral Adaptation.
973 *Genetics*. 2016;202: 285–295. doi:10.1534/genetics.115.181628
- 974 19. Wittkopp PJ, Haerum BK, Clark AG. Regulatory changes underlying expression
975 differences within and between *Drosophila* species. *Nat Genet*. Nature Publishing
976 Group; 2008;40: 346–350. doi:10.1038/ng.77
- 977 20. Stern DL. Perspective: evolutionary developmental biology and the problem of
978 variation. *Evolution*. 2009;54: 1079. doi:10.1554/0014-
979 3820(2000)054[1079:PEDBAT]2.0.CO;2
- 980 21. He X, Zhang J. Toward a Molecular Understanding of Pleiotropy. *Genetics*.
981 *Genetics*; 2006;173: 1885–1891. doi:10.1534/genetics.106.060269

- 982 22. Papakostas S, Vøllestad LA, Bruneaux M, Aykanat T, Vanoverbeke J, Ning M, et
983 al. Gene pleiotropy constrains gene expression changes in fish adapted to different
984 thermal conditions. *Nat Commun.* Nature Publishing Group; 2014;5: 4071.
985 doi:10.1038/ncomms5071
- 986 23. Altenberg L. Modularity in Evolution: Some Low-Level Questions. In: Rasskin-
987 Gutman D, Callebaut W, editors. *Modularity*. 2005.
- 988 24. Wagner GP, Altenberg L. Perspective: Complex Adaptations and the Evolution of
989 Evolvability. *Evolution*. 1996;50: 967. doi:10.2307/2410639
- 990 25. Welch JJ, Waxman D. Modularity and the cost of complexity. *Evolution*. 2003;57:
991 1723–1734.
- 992 26. Wagner GP, Pavlicev M, Cheverud JM. The road to modularity. *Nat Rev Genet.*
993 Nature Publishing Group; 2007;8: 921–931. doi:10.1038/nrg2267
- 994 27. Melo D, Porto A, Cheverud JM, Marroig G. Modularity: genes, development and
995 evolution. *Annu Rev Ecol Evol Syst.* Annual Reviews; 2016;47: 463–486.
996 doi:10.1146/annurev-ecolsys-121415-032409
- 997 28. Collet JM, McGuigan K, Allen SL, Chenoweth SF, Blows MW. Mutational
998 Pleiotropy and the Strength of Stabilizing Selection Within and Between
999 Functional Modules of Gene Expression. *Genetics*. 2018;208: 1601–1616.
1000 doi:10.1534/genetics.118.300776
- 1001 29. Paaby AB, Rockman MV. Pleiotropy: what do you mean? Reply to Zhang and
1002 Wagner. *Trends Genet.* Elsevier; 2013;29: 384. doi:10.1016/j.tig.2013.05.003
- 1003 30. Wagner GP, Zhang J. Universal pleiotropy is not a valid null hypothesis: reply to
1004 Hill and Zhang. *Nat Rev Genet.* Nature Publishing Group; 2012;13: 296–296.
1005 doi:10.1038/nrg2949-c2
- 1006 31. Hill WG, Zhang X-S. Assessing pleiotropy and its evolutionary consequences:
1007 pleiotropy is not necessarily limited, nor need it hinder the evolution of
1008 complexity. *Nat Rev Genet.* Nature Publishing Group; 2012;13: 296–296.
1009 doi:10.1038/nrg2949-c1
- 1010 32. Zhang J, Wagner GP. On the definition and measurement of pleiotropy. *Trends*
1011 *Genet.* 2013.
- 1012 33. Gibson G. Decanalization and the origin of complex disease. *Nat Rev Genet.*
1013 2009;10: 134–140. doi:10.1038/nrg2502
- 1014 34. Nuzhdin SV, Friesen ML, McIntyre LM. Genotype-phenotype mapping in a post-
1015 GWAS world. *Trends Genet.* 2012;28: 421–426. doi:10.1016/j.tig.2012.06.003

- 1016 35. Li Y, Venkataram S, agarwala A, dunn B, Petrov DA, Sherlock G, et al. Hidden
1017 Complexity of Yeast Adaptation under Simple Evolutionary Conditions. *Curr Biol.*
1018 2018;28: 515–525.e6. doi:10.1016/j.cub.2018.01.009
- 1019 36. Gorter FA, Aarts MGM, Zwaan BJ, de Visser JAGM. Local Fitness Landscapes
1020 Predict Yeast Evolutionary Dynamics in Directionally Changing Environments.
1021 *Genetics.* 2018;208: 307–322. doi:10.1534/genetics.117.300519
- 1022 37. Baym M, Stone LK, Kishony R. Multidrug evolutionary strategies to reverse
1023 antibiotic resistance. *Science.* 2016;351: aad3292–aad3292.
1024 doi:10.1126/science.aad3292
- 1025 38. Hartley SW, Monti S, Liu C-T, Steinberg MH, Sebastiani P. Bayesian methods for
1026 multivariate modeling of pleiotropic SNP associations and genetic risk prediction.
1027 *Front Genet. Frontiers;* 2012;3: 176. doi:10.3389/fgene.2012.00176
- 1028 39. Chen G, Mulla WA, Kucharavy A, Tsai H-J, Rubinstein B, Conkright J, et al.
1029 Targeting the adaptability of heterogeneous aneuploids. *Cell. Elsevier;* 2015;160:
1030 771–784. doi:10.1016/j.cell.2015.01.026
- 1031 40. Nichol D, Jeavons P, Fletcher AG, Bonomo RA, Maini PK, Paul JL, et al. Steering
1032 Evolution with Sequential Therapy to Prevent the Emergence of Bacterial
1033 Antibiotic Resistance. *PLoS Comput Biol.* 2015;11: e1004493.
1034 doi:10.1371/journal.pcbi.1004493
- 1035 41. Kaznatcheev A, Peacock J, Basanta D, Marusyk A, Scott JG. Fibroblasts and
1036 alectinib switch the evolutionary games played by non-small cell lung cancer. *Nat*
1037 *Ecol Evol.* 2019;3: 450–456. doi:10.1038/s41559-018-0768-z
- 1038 42. Paaby AB, Rockman MV. The many faces of pleiotropy. *Trends Genet. Elsevier;*
1039 2013;29: 66–73. doi:10.1016/j.tig.2012.10.010
- 1040 43. Walsh B, Blows MW. Abundant Genetic Variation + Strong Selection =
1041 Multivariate Genetic Constraints: A Geometric View of Adaptation.
1042 <http://dxdoiorg/101146/annurevecolsys110308120232>. *Annual Reviews;* 2009;40:
1043 41–59. doi:10.1146/annurev.ecolsys.110308.120232
- 1044 44. Ference BA, Ginsberg HN, Graham I, Ray KK, Packard CJ, Bruckert E, et al.
1045 Low-density lipoproteins cause atherosclerotic cardiovascular disease. 1. Evidence
1046 from genetic, epidemiologic, and clinical studies. A consensus statement from the
1047 European Atherosclerosis Society Consensus Panel. *Eur Heart J.* 2017;38: 2459–
1048 2472. doi:10.1093/eurheartj/ehx144
- 1049 45. Hafid Al N, Christodoulou J. Phenylketonuria: a review of current and future
1050 treatments. *Transl Pediatr.* 2015;4: 304–317. doi:10.3978/j.issn.2224-
1051 4336.2015.10.07

- 1052 46. Powell ALT, Nguyen CV, Hill T, Cheng KL, Figueroa-Balderas R, Aktas H, et al.
1053 Uniform ripening encodes a Golden 2-like transcription factor regulating tomato
1054 fruit chloroplast development. *Science*. 2012;336: 1711–1715.
1055 doi:10.1126/science.1222218
- 1056 47. Grüneberg H. An analysis of the “pleiotropic” effects of a new lethal mutation in
1057 the rat (*Mus norvegicus*). 1938. doi:10.2307/82266
- 1058 48. Ohya Y, Sese J, Yukawa M, Sano F, Nakatani Y, Saito TL, et al. High-
1059 dimensional and large-scale phenotyping of yeast mutants. *Proceedings of the*
1060 *National Academy of Sciences*. 2005;102: 19015–19020.
1061 doi:10.1073/pnas.0509436102
- 1062 49. Bauer CR, Li S, Siegal ML. Essential gene disruptions reveal complex
1063 relationships between phenotypic robustness, pleiotropy, and fitness. *Mol Syst*
1064 *Biol*. 2015;11: 773–773. doi:10.15252/msb.20145264
- 1065 50. Geiler-Samerotte KA, Zhu YO, Goulet BE, Hall DW, Siegal ML. Selection
1066 Transforms the Landscape of Genetic Variation Interacting with Hsp90. *PLoS*
1067 *Biol*. 2016;14: e2000465. doi:10.1371/journal.pbio.2000465
- 1068 51. Richardson JB, Uppendahl LD, Traficante MK, Levy SF, Siegal ML. Histone
1069 variant HTZ1 shows extensive epistasis with, but does not increase robustness to,
1070 new mutations. *PLoS Genet*. 2013;9: e1003733. doi:10.1371/journal.pgen.1003733
- 1071 52. Negishi T, Nogami S, Ohya Y. Multidimensional quantification of subcellular
1072 morphology of *Saccharomyces cerevisiae* using CalMorph, the high-throughput
1073 image-processing program. *J Biotechnol*. 2009;141: 109–117.
1074 doi:10.1016/j.jbiotec.2009.03.014
- 1075 53. Gerke J, Lorenz K, Cohen B. Genetic interactions between transcription factors
1076 cause natural variation in yeast. *Science*. 2009;323: 498–501.
1077 doi:10.1126/science.1166426
- 1078 54. Hall DW, Mahmoudizad R, Hurd AW, Joseph SB. Spontaneous mutations in
1079 diploid *Saccharomyces cerevisiae*: another thousand cell generations. *Genet Res*
1080 2008;90: 229–241. doi:10.1017/S0016672308009324
- 1081 55. Zhu YO, Siegal ML, Hall DW, Petrov DA. Precise estimates of mutation rate and
1082 spectrum in yeast. *Proc Natl Acad Sci USA*. 2014;111: E2310–8.
1083 doi:10.1073/pnas.1323011111
- 1084 56. Cooper TF, Ostrowski EA, Travisano M. A negative relationship between
1085 mutation pleiotropy and fitness effect in yeast. *Evolution*. 2007;61: 1495–1499.
1086 doi:10.1111/j.1558-5646.2007.00109.x

- 1087 57. Yang M, Ohnuki S, Ohya Y. Unveiling nonessential gene deletions that confer
1088 significant morphological phenotypes beyond natural yeast strains. *BMC*
1089 *Genomics*. 2014;15: 932. doi:10.1186/1471-2164-15-932
- 1090 58. Sahai E. Mechanisms of cancer cell invasion. *Curr Opin Genet Dev*. 2005;15: 87–
1091 96. doi:10.1016/j.gde.2004.12.002
- 1092 59. Gerke JP, Chen CTL, Cohen BA. Natural isolates of *Saccharomyces cerevisiae*
1093 display complex genetic variation in sporulation efficiency. *Genetics*. 2006;174:
1094 985–997. doi:10.1534/genetics.106.058453
- 1095 60. Liti G, Carter DM, Moses AM, Warringer J, Parts L, James SA, et al. Population
1096 genomics of domestic and wild yeasts. *Nature*. 2009;458: 337–341.
1097 doi:10.1038/nature07743
- 1098 61. Skelly DA, Merrihew GE, Riffle M, Connelly CF, Kerr EO, Johansson M, et al.
1099 Integrative phenomics reveals insight into the structure of phenotypic diversity in
1100 budding yeast. *Genome Res*. 2013;23: 1496–1504. doi:10.1101/gr.155762.113
- 1101 62. Ziv N, Shuster BM, Siegal ML, Gresham D. Resolving the Complex Genetic Basis
1102 of Phenotypic Variation and Variability of Cellular Growth. *Genetics*. 2017;
1103 genetics.116.195180. doi:10.1534/genetics.116.195180
- 1104 63. Broman KW, Wu H, Sen S, Churchill GA. R/qtl: QTL mapping in experimental
1105 crosses. *Bioinformatics*. 2003;19: 889–890.
- 1106 64. Stuckey S, Storici F. Gene knockouts, in vivo site-directed mutagenesis and other
1107 modifications using the delitto perfetto system in *Saccharomyces cerevisiae*. *Meth*
1108 *Enzymol*. 2013;533: 103–131. doi:10.1016/B978-0-12-420067-8.00008-8
- 1109 65. Cherry JM, Hong EL, Amundsen C, Balakrishnan R, Binkley G, Chan ET, et al.
1110 *Saccharomyces* Genome Database: the genomics resource of budding yeast.
1111 *Nucleic Acids Res*. 2012;40: D700–5. doi:10.1093/nar/gkr1029
- 1112 66. Graziano BR, Yu H-YE, Alioto SL, Eskin JA, Ydenberg CA, Waterman DP, et al.
1113 The F-BAR protein Hof1 tunes formin activity to sculpt actin cables during
1114 polarized growth. *Mol Biol Cell*. 2014;25: 1730–1743. doi:10.1091/mbc.E14-03-
1115 0850
- 1116 67. Nogami S, Ohya Y, Yvert G. Genetic Complexity and Quantitative Trait Loci
1117 Mapping of Yeast Morphological Traits. *PLoS Genet*. 2007;3: e31.
1118 doi:10.1371/journal.pgen.0030031
- 1119 68. Lynch M, Walsh B. Correlations between characters. *Genetics and Analysis of*
1120 *Quantitative Traits*. Sinauer Associates Incorporated; 1998. pp. 629–656.
1121 doi:10.1046/j.1420-9101.2003.00556.x/full
- 1122 69. Bliese P. Multilevel modeling in R (2.5). Retrieved September 2013.

- 1123 70. Breiman L, Friedman JH. Estimating Optimal Transformations for Multiple
1124 Regression and Correlation. *Journal of the American Statistical Association*.
1125 Taylor & Francis Group; 2012;80: 580–598.
- 1126 71. Setty M, Tadmor MD, Reich-Zeliger S, Angel O, Salame TM, Kathail P, et al.
1127 Wishbone identifies bifurcating developmental trajectories from single-cell data.
1128 *Nat Biotechnol*. 2016;34: 637–645. doi:10.1038/nbt.3569
- 1129 72. Turner JJ, Ewald JC, Skotheim JM. Cell size control in yeast. *Curr Biol*. 2012;22:
1130 R350–9. doi:10.1016/j.cub.2012.02.041
- 1131 73. Wang R, Kamgoue A, Normand C, Léger-Silvestre I, Mangeat T, Gadal O. High
1132 resolution microscopy reveals the nuclear shape of budding yeast during cell cycle
1133 and in various biological states. *J Cell Sci*. 2016;129: 4480–4495.
1134 doi:10.1242/jcs.188250
- 1135 74. Logg K, Bodvard K, Blomberg A, Käll M. Investigations on light-induced stress in
1136 fluorescence microscopy using nuclear localization of the transcription factor
1137 Msn2p as a reporter. *FEMS Yeast Res*. 2009;9: 875–884. doi:10.1111/j.1567-
1138 1364.2009.00536.x
- 1139 75. Wickham H. *ggplot2*. New York, NY: Springer New York; 2009.
1140 doi:10.1007/978-0-387-98141-3
- 1141 76. Pavlicev M, Cheverud JM. Constraints Evolve: Context Dependency of Gene
1142 Effects Allows Evolution of Pleiotropy. *Annu Rev Ecol Evol Syst*. 2015;46:
1143 413:434.
- 1144 77. Pavlicev M, Wagner GP, Noonan JP, Hallgrímsson B, Cheverud JM. Genomic
1145 correlates of relationship QTL involved in fore- versus hind limb divergence in
1146 mice. *Genome Biol Evol*. 2013;5: 1926–1936. doi:10.1093/gbe/evt144
- 1147 78. Porto A, Schmelter R, VandeBerg JL, Marroig G, Cheverud JM. Evolution of the
1148 genotype-to-phenotype map and the cost of pleiotropy in mammals. *Genetics*.
1149 2016;204: 1601–1612.
- 1150 79. Lande R. Quantitative genetic analysis of multivariate evolution, applied to
1151 brain:body size allometry. *Evolution*. 2017;33: 402–416. doi:10.1111/j.1558-
1152 5646.1979.tb04694.x
- 1153 80. Arnold SJ, Bürger R, Hohenlohe PA, Ajie BC, Jones AG. Understanding the
1154 evolution and stability of the g-matrix. *Evolution*. 2008;62: 2451–2461.
1155 doi:10.1111/j.1558-5646.2008.00472.x
- 1156 81. Björklund M, Husby A, Gustafsson L. Rapid and unpredictable changes of the G-
1157 matrix in a natural bird population over 25 years. *J Evol Biol*. 2012;26: 1–13.
1158 doi:10.1111/jeb.12044

- 1159 82. Cheverud JM. A comparison of genetic and phenotypic correlations. *Evolution*.
1160 2017;42: 958–968. doi:10.1111/j.1558-5646.1988.tb02514.x
- 1161 83. Arnold SJ, Phillips PC. Hierarchical comparison of genetic variance-covariance
1162 matrices. II coastal-inland divergence in the garter snake, *Thamnophis elegans*.
1163 *Evolution*. 2017;53: 1516–1527. doi:10.1111/j.1558-5646.1999.tb05415.x
- 1164 84. Sgrò CM, Hoffmann AA. Genetic correlations, tradeoffs and environmental
1165 variation. *Heredity*. 2004;93: 241–248.
- 1166 85. Pavlicev M, Wagner GP. Evolutionary Systems Biology: Shifting Focus to the
1167 Context-Dependency of Genetic Effects. *Integrative Organismal Biology*. 2015. p.
1168 91:108.
- 1169 86. Levy SF, Siegal ML. Network hubs buffer environmental variation in
1170 *Saccharomyces cerevisiae*. *PLoS Biol*. 2008;6: e264.
1171 doi:10.1371/journal.pbio.0060264
- 1172 87. Ziv N, Siegal ML, Gresham D. Genetic and nongenetic determinants of cell
1173 growth variation assessed by high-throughput microscopy. *Mol Biol Evol*.
1174 2013;30: 2568–2578. doi:10.1093/molbev/mst138
- 1175 88. Millard SP. *EnvStats*. New York, NY: Springer Science & Business Media; 2013.
1176 doi:10.1007/978-1-4614-8456-1
- 1177 89. Gietz RD, Woods RA. Transformation of yeast by lithium acetate/single-stranded
1178 carrier DNA/polyethylene glycol method. *Meth Enzymol*. 2002;350: 87–96.
- 1179 90. Miyajima I, Nakafuku M, Nakayama N, Brenner C, Miyajima A, Kaibuchi K, et
1180 al. GPA1, a haploid-specific essential gene, encodes a yeast homolog of
1181 mammalian G protein which may be involved in mating factor signal transduction.
1182 *Cell*. 1987;50: 1011–1019.
- 1183 91. Pinheiro J, Bates D, DebRoy S, Sarkar D. R Core Team (2018). *nlme: linear and*
1184 *nonlinear mixed effects models*. R package version 3.1-137. 2018.
- 1185 92. Levy SF, Ziv N, Siegal ML. Bet hedging in yeast by heterogeneous, age-correlated
1186 expression of a stress protectant. *PLoS Biol*. 2012;10: e1001325.
1187 doi:10.1371/journal.pbio.1001325
- 1188 93. Li S, Giardina DM, Siegal ML. Control of nongenetic heterogeneity in growth rate
1189 and stress tolerance of *Saccharomyces cerevisiae* by cyclic AMP-regulated
1190 transcription factors. *PLoS Genet*. 2018;14: e1007744.
1191 doi:10.1371/journal.pgen.1007744

Figures:

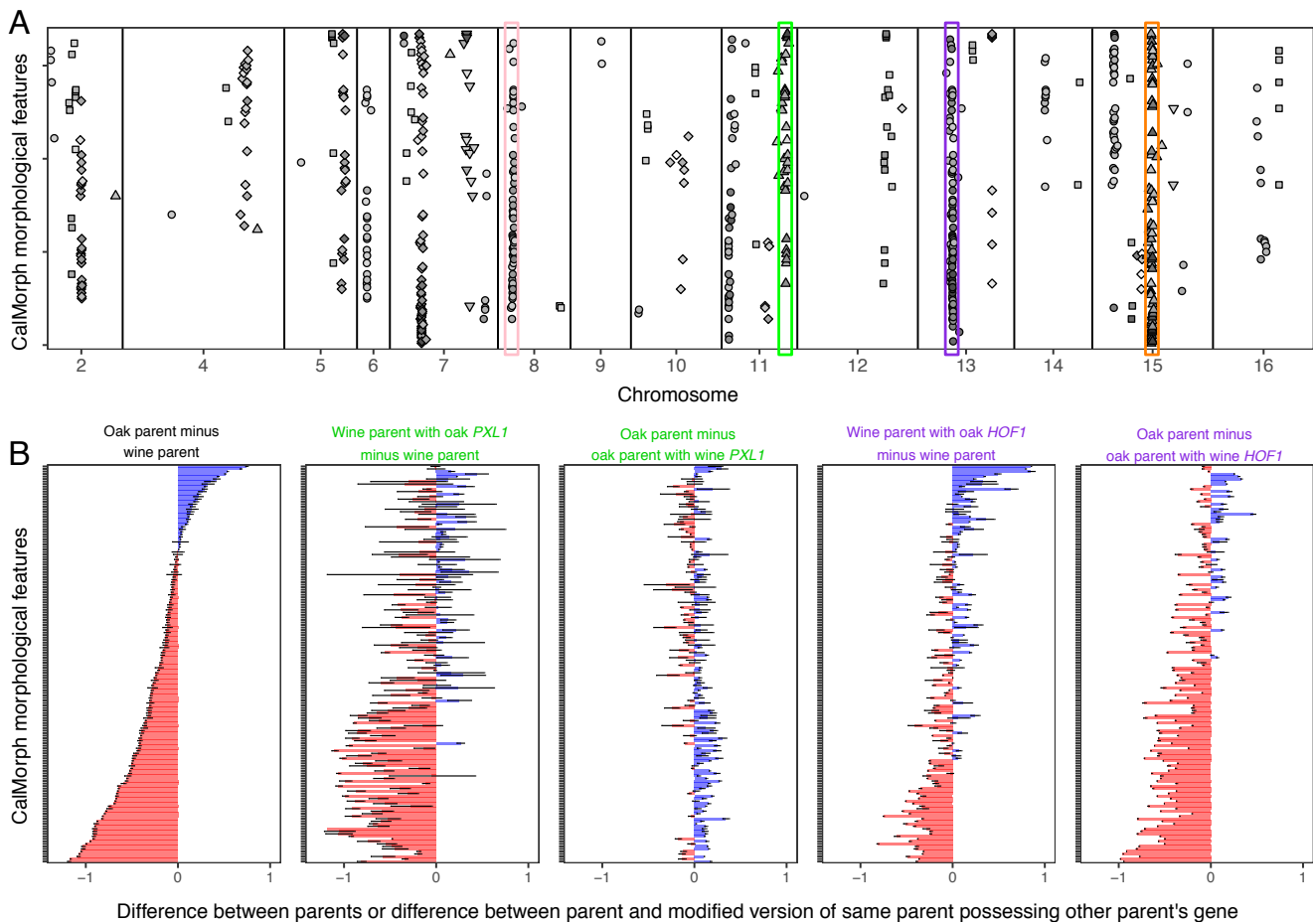


Figure 1: Pleiotropic QTL influence yeast single-cell morphology. The vertical axes in all plots represent the 158 CalMorph morphological traits for which we detect QTL with a genome-wide FDR of 5%. These traits are sorted, from top to bottom, based on the difference between the oak and wine parental strains. **(A)** Of 44 QTL that contribute to variation in single-cell morphology, 37 contribute to variation in multiple features. The horizontal axis indicates the chromosomal location of each QTL (in cM). Differently shaped points indicate QTL that are more than 30 cM apart on the same chromosome. The darkness of a point represents the effect size of a QTL; effect sizes range from 0.3% (lightest points) to 18% (darkest points) of the difference between parents. The QTL highlighted in pink, green, purple, and orange contribute to 58, 33, 78, or 66 morphological features, respectively. **(B)** Single genes contribute to multiple morphological features. The horizontal axis represents the relative phenotypic differences between the wine and oak parents (leftmost column) or one of these strains versus a derivative strain that differs in a single gene. The relative phenotypic differences between a pair of strains are calculated by scaling each trait to have a mean of 0 and standard deviation of 1 across all individuals in both strains, and then subtracting the average value in one strain from that in the other. To control for variation among replicate experiments, this scaling was done independently for each replicate experiment in which both strains were imaged. Error bars represent 95% confidence intervals inferred from the replicate experiments. The two gene replacements shown, *PXL1* and *HOF1*, are respectively located within the QTL highlighted in green and purple in panel A. When calculating the difference between strains, we always subtracted the trait values of the strain possessing more wine genes from those of the strain possessing more oak genes, such that the effects of the wine or oak gene replacements appear in the same direction on all plots.

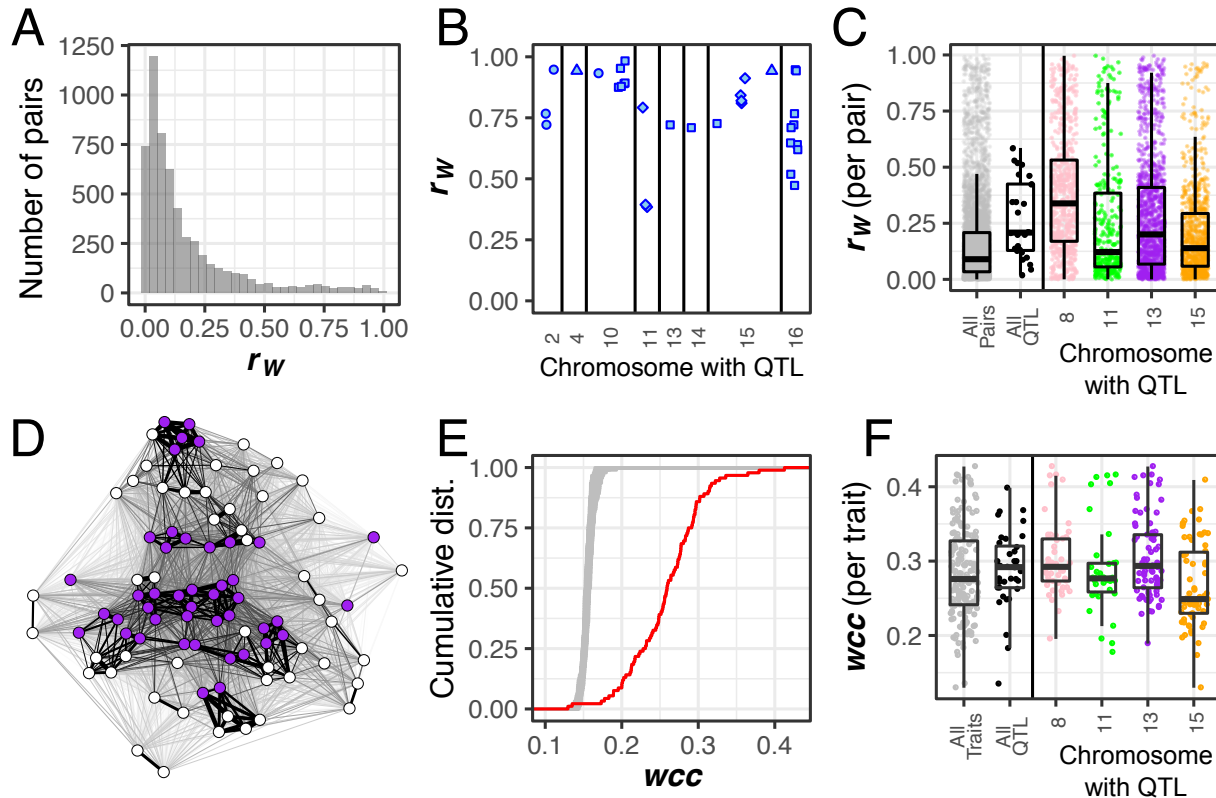


Figure 2: Pairs of traits with high correlation across clones are overrepresented among those influenced by pleiotropic QTL. Within-genotype correlations (r_w) are calculated for 5645 pairs of morphological traits. **(A)** Histogram showing distribution of r_w . **(B)** This plot displays the 11 of 35 pleiotropic QTL that exclusively influence pairs of traits with $r_w > 0.2$. Points represent r_w for pairs of traits influenced by a QTL; the shapes of these points match those in **Fig 1A** and distinguish a QTL from others on the same chromosome. **(C)** Points in grey represent r_w for all 5645 pairs of traits. Points in black each represent the median r_w across pairs of traits influenced by one of the 24 pleiotropic QTL not included in panel B. The next four sets of points each display r_w for pairs of traits influenced by a single QTL corresponding to those highlighted in the same color in **Fig 1A**. Each boxplot shows the median (center line), interquartile range (IQR) (upper and lower hinges), and highest value within $1.5 \times \text{IQR}$ (whiskers). **(D)** A force-directed network visualizing how pairs of morphological features correlate across clones. Each node represents a single-cell morphological trait measured in large-budded cells. The thickness of the line connecting each pair of nodes is proportional to r_w . Node position in the network is determined using the Fruchterman-Reingold algorithm. Purple nodes correspond to traits influenced by a QTL on chromosome 13 containing the *HOF1* gene. **(E)** Cumulative distributions of weighted clustering coefficients (wcc) in a network created using measured values of r_w (red line) or in 100 permuted networks (grey lines) for traits corresponding to large-budded cells. Permutations were performed by sampling r_w , without replacement, and reassigning each value to a random pair of traits. **(F)** This panel is similar to panel C, except points represent wcc of traits rather than r_w of trait pairs, and black points each represent the median wcc across traits influenced by one of 24 pleiotropic QTL.

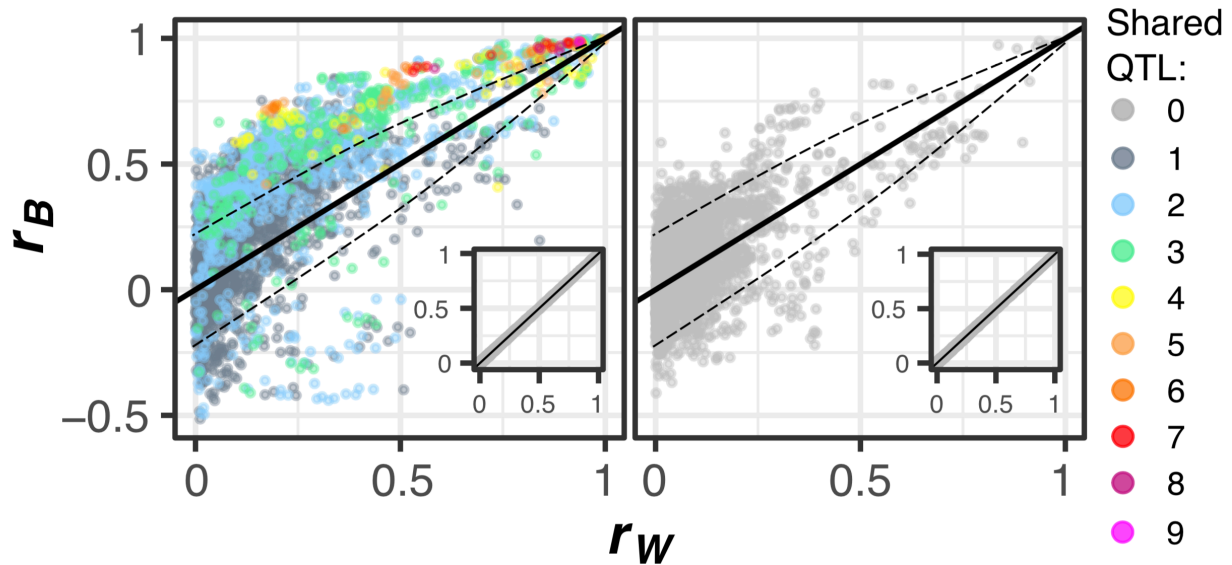


Figure 3: Natural genetic variation affects the correlation between morphological features. The absolute value of the between-strain correlation (r_B), made negative when r_B and r_W have opposite signs, is plotted against the absolute value of the within-strain correlation (r_W), for each pair of traits. The plot at left shows pairs of traits that share at least one QTL influence. The color of each point represents the number of pleiotropic QTL that influence both traits in that pair. The plot at right shows pairs of traits that share no QTL influence. The dashed line represents a Bonferroni-corrected significance threshold of $p < 0.01$. Insets represent the results of correlation partitioning performed after randomly assigning individual cells to groups (pseudo-strains) having the same numbers of cells as the actual strains.

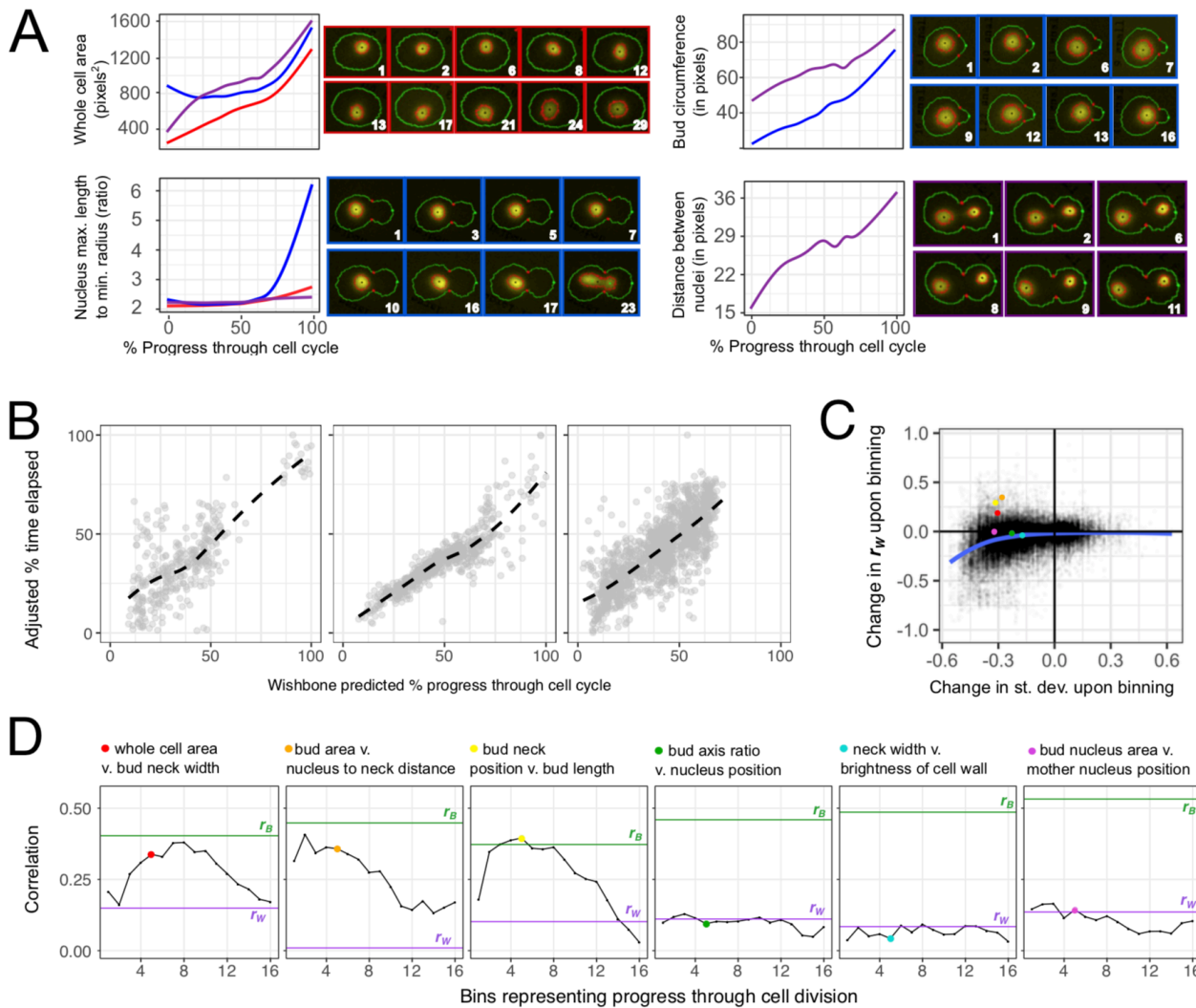


Figure 4: Morphological features vary as cells divide. The morphological features of unbudded (red), small-budded (blue), and large-budded (purple) cells change as these cells progress through the cell cycle. **(A)** Variation of four traits through the cell cycle. Line plots represent fixed-cell images from all 374 mapping family strains, positioned on the horizontal axis based on progression through the cell cycle as calculated by Wishbone [71]. Regression lines are smoothed with cubic splines, calculated with the “gam” method in the R package ggplot2 [75], to depict trends describing how each displayed trait varies across the estimated growth trajectory. The displayed trends match those observed in micrographs of live cells progressing through division. Each series of micrographs displays a different live cell imaged over several minutes, which are displayed in the lower right corner of each micrograph. **(B)** Centered data for 11, 23, and 44 unbudded, small-budded and large-budded cells, respectively, show how Wishbone sorts live cells in a way that recapitulates the actual time series. Each point in these plots represents a cell image from a single timepoint. The horizontal axis represents Wishbone’s estimation of how far that cell has progressed through division. The vertical axis displays time, as a percentage of the total time elapsed and adjusted in a way that controls for every cell having started at a different place in the cell division cycle at time zero (see *Methods*). Trend lines are smooth fits using the “loess” method in the R package ggplot [75]. **(C)** The correlation between some morphological features changes throughout the course of cell division. The scatterplot shows how binning influences both the phenotypic correlation (vertical axis) and phenotypic variation (horizontal axis) across clones. Each point represents these values for a pair of traits as

measured in 1 of 16 bins. The value on the horizontal axis represents whichever trait in each pair had the larger decrease in standard deviation, as such decreases are likely to reduce the correlation on the vertical axis. The blue line shows a smooth fit by loess regression. Colored points on the scatterplot correspond to bin 5 for each pair of traits represented by the line plots in panel **D**. (**D**) These line plots show three pairs of traits for which binning increases r_W such that it approaches r_B (leftmost three plots), and three pairs of traits for which r_W does not approach r_B even after binning (rightmost three plots). In each plot, r_B is shown as the horizontal green line, r_W (without binning) is shown as the horizontal purple line, and r_W for each bin is shown in black.

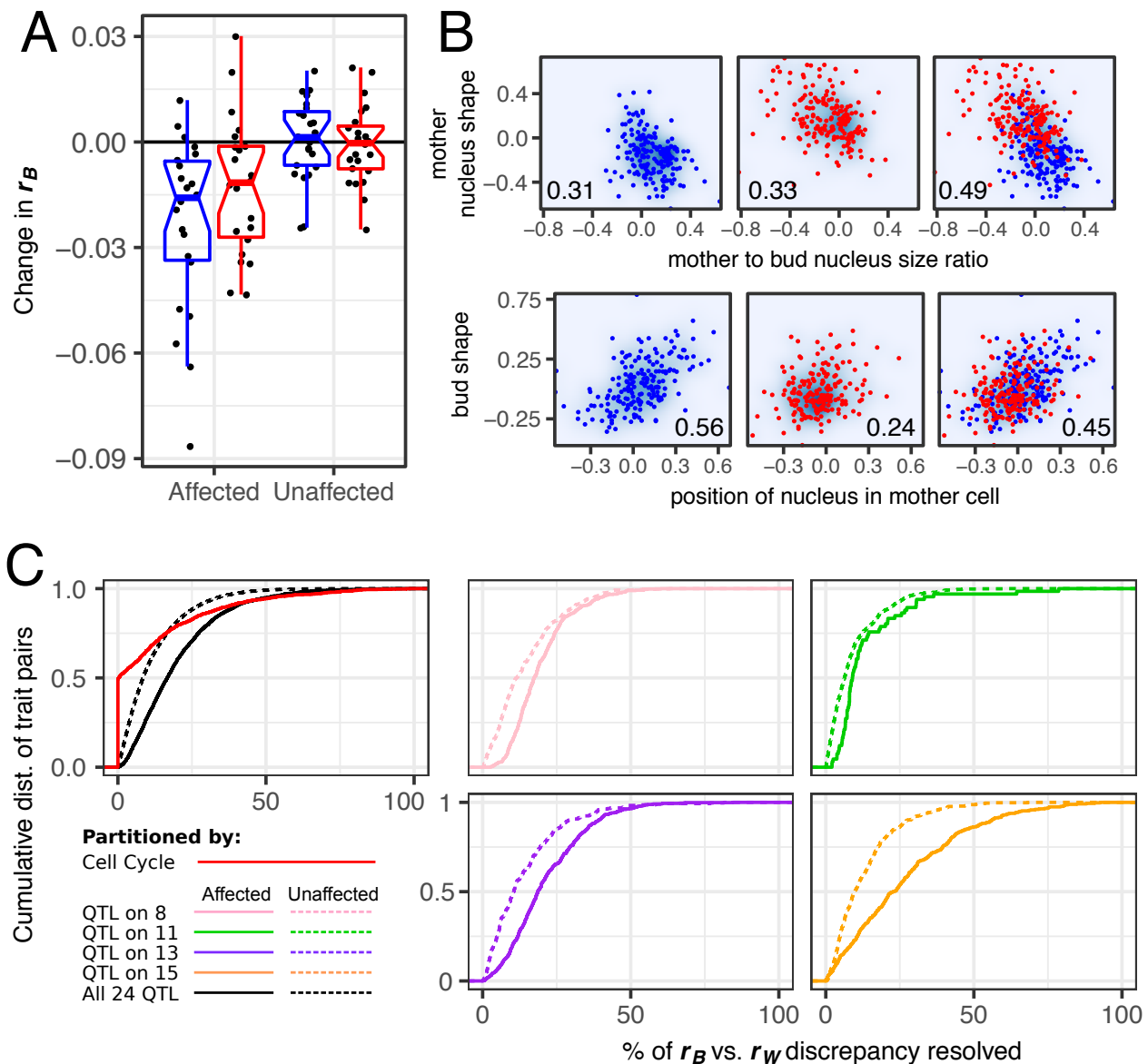


Figure 5: Many QTL demonstrate horizontal pleiotropy. (A) Eliminating allelic variation at the site of each QTL tends to reduce r_B . The vertical axis represents how r_B changes upon eliminating allelic variation at each QTL site. Each point represents the median change in r_B for all pairs of traits that are affected or unaffected by one of the 24 QTL suspected of horizontal pleiotropy. Boxplots summarize these changes in r_B when re-measured across strains possessing the wine (red) or the oak (blue) allele at the marker closest to the QTL. (B) The upper and lower series of three plots demonstrate two different ways that a QTL can increase the correlation between traits. Each point represents a yeast strain possessing either the wine (red) or the oak (blue) allele at a marker closest to a QTL on chromosome 15 (upper) or 8 (lower). In the upper plots, the QTL increases the correlation between nucleus shape and size ratio when it is segregating across strains. In the lower plots, the wine allele strengthens a correlation between bud shape and the position of the nucleus in the mother cell that is weak in the oak subpopulation. Numbers in the lower corner of each plot represent r_B for the strains displayed. (C) Cumulative distributions display the extent to which binning cells or splitting strains resolves the difference between r_B and r_W . When calculating percent resolved (horizontal axes) we always plot the value in whichever

subset (*e.g.* wine or oak) this percent is greatest. If subsetting always worsens the discrepancy between r_B vs. r_W , we score this as 0% resolution. Only pairs of traits for which r_B is significantly greater than r_W are considered. The pink, green, purple and orange lines show the effect of splitting strains by whether they inherited the wine or oak allele at the marker closest to each of four QTL (colors correspond to QTL in **Fig 1A**). In these plots, comparing the solid vs dotted lines shows that splitting strains resolves the discrepancy between r_B and r_W more often for pairs in which both traits are affected by the QTL than pairs in which both traits are unaffected. The black lines in the leftmost plot summarize these effects across 24 QTL, displaying for each trait pair, the largest resolution in the r_B vs. r_W discrepancy observed across all QTL that affect the pair of traits (solid line) or all QTL that do not (dotted line). The red line shows the effect of binning cells by their progress through division, displaying the largest resolution in the r_B vs. r_W difference across all 16 bins.

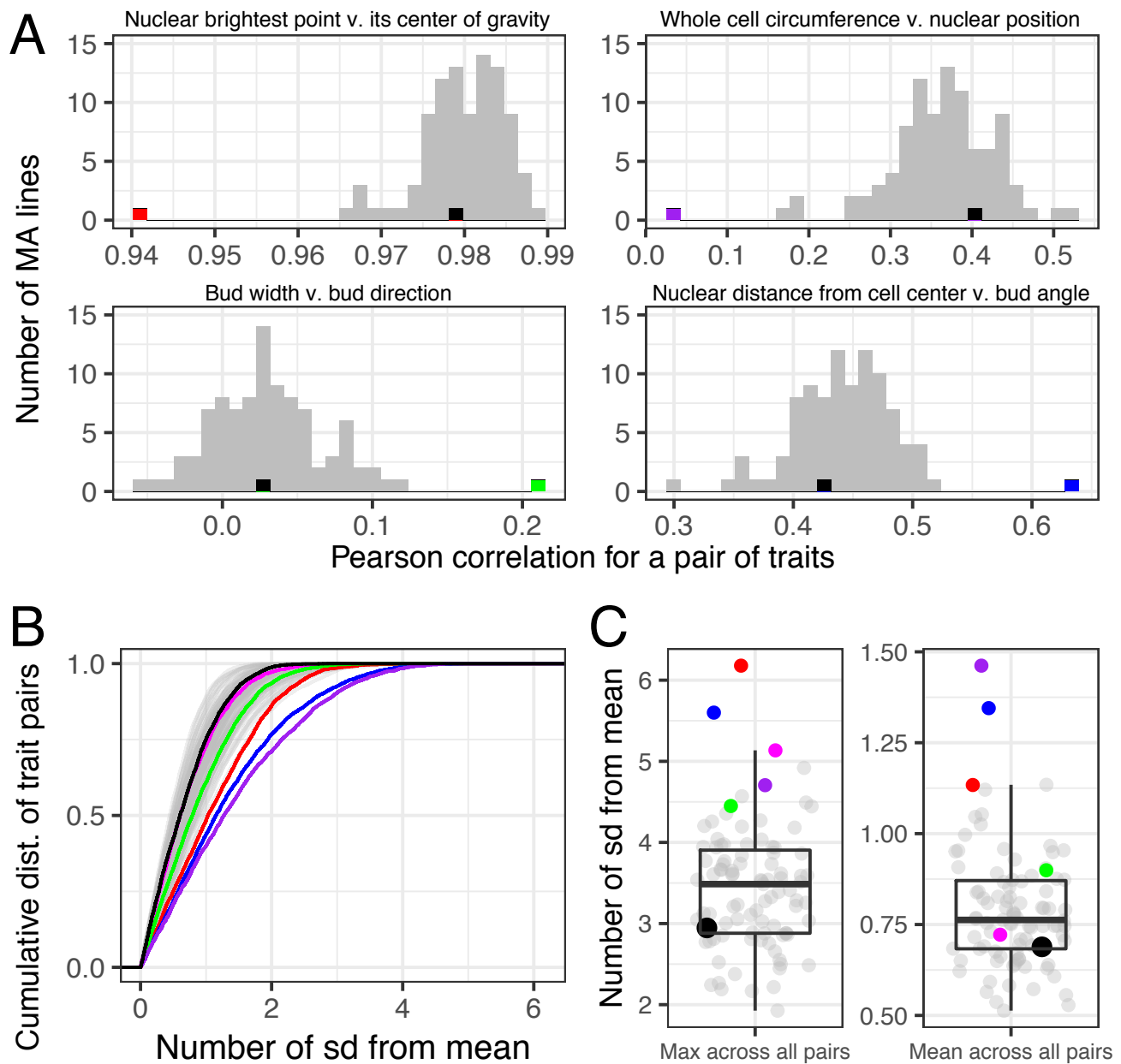


Figure 6: Some MA lines display unique relationships between certain pairs of traits. In all plots, black represents the ancestor of the MA lines and colors represent MA lines with trait correlations that differ from other lines (strains: black = HAncestor, green = DHC81H1, red = DHC41H1, magenta = DHC40H1, blue = DHC66H1, purple = DHC84H1; see Table S2 in Geiler-Samerotte et al 2016 [50]). **(A)** Histograms display the number of MA lines with Pearson correlations corresponding to the values on the horizontal axis for four example pairs of traits; the number of bins is set to 30. **(B)** This plot displays, for each of the 94 MA lines, the cumulative distribution of the number of standard deviations away from the mean correlation across all trait pairs. **(C)** Plots display, for each MA line, the maximum deviation from the mean observed for any pair of traits (left) and the average standard deviation observed across all pairs of traits (right).

Supplemental Figures:

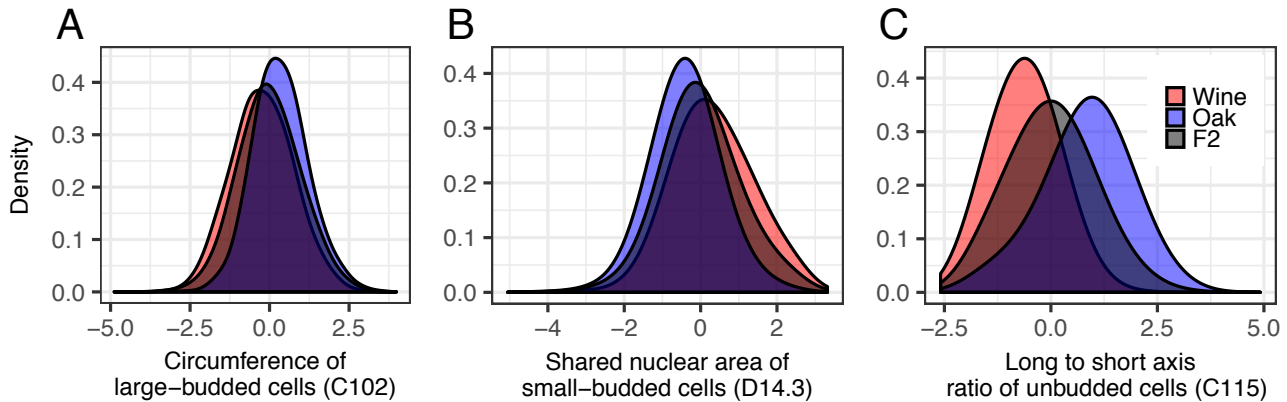


Figure S1: Morphological differences exist between the parents of the QTL mapping family. Each density plot displays the distribution of phenotype values from yeast cells corresponding to the wine parent (red), the oak parent (blue), or all of the 374 progeny (grey) for the trait listed on the horizontal axis. Trait names in parentheses correspond to those listed in the CalMorph manual [52]. Before plotting, each morphological trait was transformed to have a mean of zero and a standard deviation of one across all strains. Each distribution represents at minimum 5,000 cells from three replicate experiments; distributions corresponding to progeny strains represent many more cells (70,000 – 200,000 depending on whether the trait was measured in unbudded, small-budded, or large-budded cells).

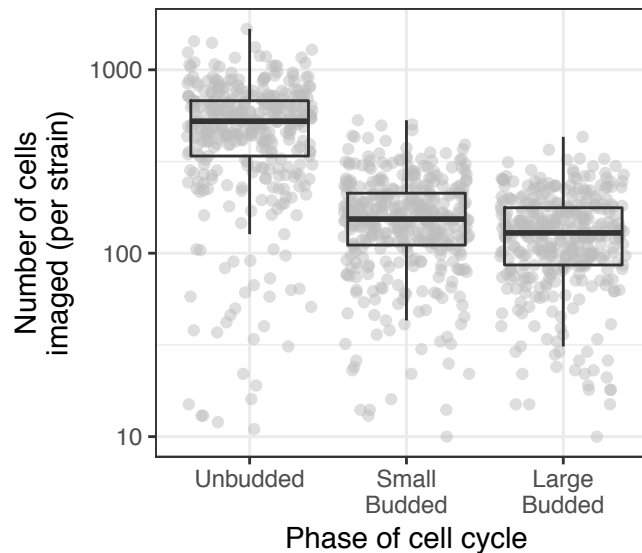


Figure S2: Total numbers of cells imaged per each of 374 progeny strains. Each point represents, for one of the 374 progeny strains, the number of unbudded, small-budded, or large-budded cells for which images passed filtering (see *Methods*). Each boxplot shows the median (center line), interquartile range (IQR) (upper and lower hinges), and highest value within $1.5 \times \text{IQR}$ (whiskers).

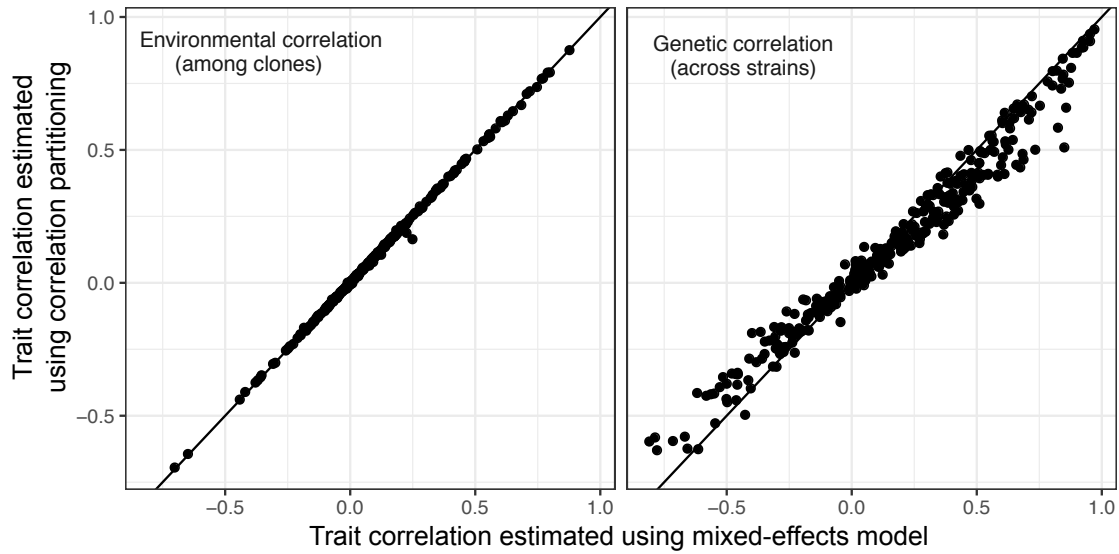


Figure S3: Comparison of correlation estimates obtained from correlation partitioning with those obtained from a mixed-effect linear model. Each point represents one of 350 randomly sampled trait pairs of the 5645 total. Vertical axes display trait correlations estimated using the correlation-partitioning approach; horizontal axes display trait correlations estimated using a mixed-effect linear model that specifies the variance-covariance structure of the experimental design.

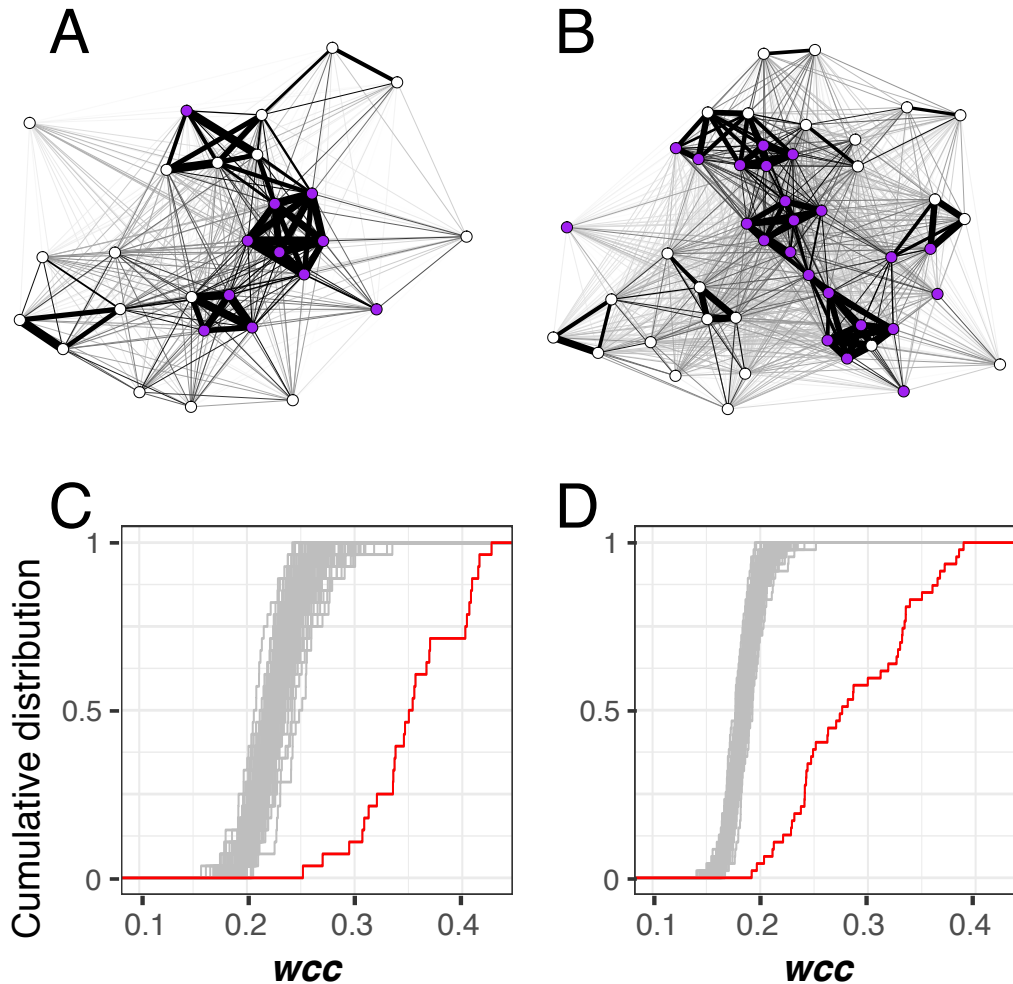


Figure S4: Single-cell morphological traits have higher weighted clustering coefficients (wcc) than expected given the distribution of r_w . (A – B) Force-directed networks visualizing how pairs of morphological features correlate across clones in unbudged (panel A) and small-budded (panel B) cells. Each node represents a single-cell morphological trait. The thickness of the line connecting each pair of nodes is proportional to r_w . Node position in the network is determined using the Fruchterman-Reingold algorithm. Purple nodes correspond to traits influenced by a QTL on chromosome 13 containing the *HOF1* gene. (C – D) Cumulative distributions of weighted clustering coefficients (wcc) in a network created using measured values of r_w (red line) or in 100 permuted networks (grey lines) for traits corresponding to unbudged (panel C) or small-budded (panel D) cells. Permutations were performed by sampling r_w , without replacement, and reassigning each value to a random pair of traits.

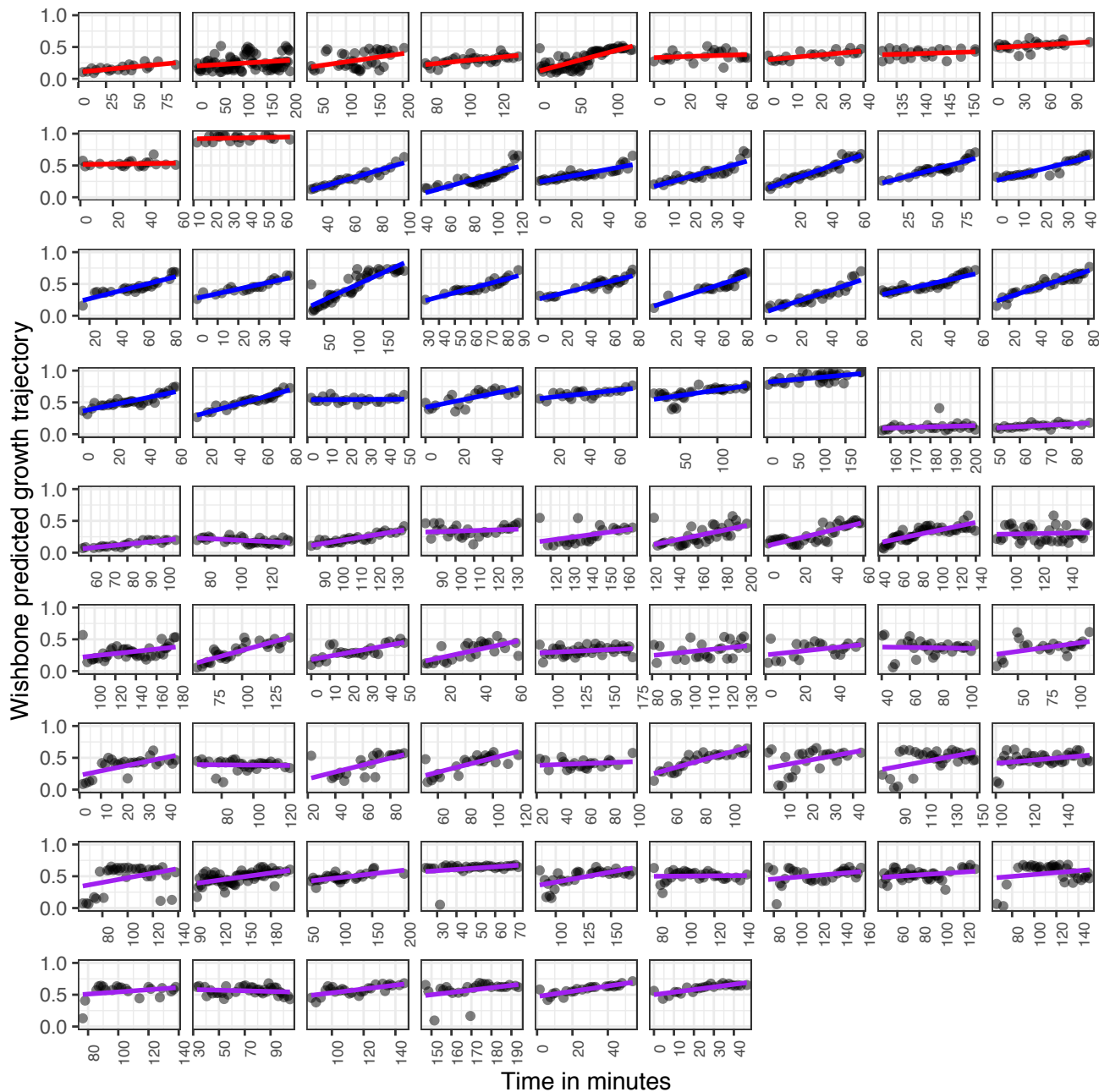


Figure S5: Wishbone recapitulates time series data obtained in live images of 78 cells undergoing exponential growth. Each point represents a cell image. Horizontal axes display the minute that image was captured during a three-hour window of exponential growth. Vertical axes display Wishbone’s prediction of how far that cell image has passed through the cell cycle. Linear regression lines are calculated with the “lm” method in the R package ggplot2 [75], and are colored red for images corresponding to unbudded cells, blue for small-budded cells and purple for large-budded cells. Plots are organized by cell type and then from earliest to latest average predicted progress through cell division.

S1 Table. Chromosomal locations, effects sizes and phenotypes affected by quantitative trait loci described in this study.

S2 Table. Impact of gene swaps on single-cell morphological traits including the corrected phenotypic difference between strains for each phenotype, and its standard deviation and standard error across replicate experiments.